Accelerated sediment delivery to continental margins during post-orogenic rebound of mountain ranges

Thomas Bernard, Hugh D Sinclair

▶ **To cite this version:**

Thomas Bernard, Hugh D Sinclair. Accelerated sediment delivery to continental margins during post-orogenic rebound of mountain ranges. Basin Research, 2022, 35 (2), pp.642-661. 10.1111/bre.12727 . insu-03843273

HAL Id: insu-03843273
https://insu.hal.science/insu-03843273

Submitted on 8 Nov 2022

HAL is a multi-disciplinary open access archive for the deposit and dissemination of scientific research documents, whether they are published or not. The documents may come from teaching and research institutions in France or abroad, or from public or private research centers.

L'archive ouverte pluridisciplinaire **HAL**, est destinée au dépôt et à la diffusion de documents scientifiques de niveau recherche, publiés ou non, émanant des établissements d'enseignement et de recherche français ou étrangers, des laboratoires publics ou privés.

Received: 10 January 2022 | Revised: 9 September 2022 | Accepted: 22 September 2022

DOI: 10.1111/bre.12727

RESEARCH ARTICLE

Basin Research | IAS EAGE | WILEY

Accelerated sediment delivery to continental margins during post-orogenic rebound of mountain ranges

Thomas Bernard[1] | **Hugh D. Sinclair**[2]

[1]Géosciences Rennes, Université de Rennes 1, Rennes, France

[2]School of Geosciences, The University of Edinburgh, Edinburgh, UK

Correspondence
Thomas Bernard, Géosciences Rennes, Université de Rennes 1, Rennes, 35000, France.
Email: bernard.thomas0192@gmail.com

Funding information
Bureau de Recherches Géologiques et Minières; Conseil National de la Recherche Scientifique; Total

Abstract

Changes in sediment flux to continental margins are commonly interpreted in terms of tectonic growth of topography or climatic change. Here, we show that variations in sediment yield from orogenic systems, previously considered as resulting from climate change, drainage reorganisation or mantle processes can be explained by intrinsic mechanisms of mountain belt/foreland basin systems naturally evolving during post-orogenic decay. Numerical modelling indicates an increase of sediment flux leaving the orogenic system synchronous with the cessation of deposition in the foreland basin and the transition from late syn- to post-orogenesis. Experiments highlight the importance of lithospheric flexure that causes the post-orogenic isostatic rebound of the foreland basin. Erosion of the rebounding foreland basin combined with continued sediment flux from the thrust wedge drives an acceleration in sediment outflux towards continental margins. Sediment budget records in natural settings such as the Northern Pyrenees or Western European Alps also indicate accelerated post-orogenic sediment delivery to the Bay of Biscay and Rhône Delta respectively. These intrinsic processes that determine sediment yield to continental margins must be accounted for prior to consideration of additional external tectonic or climatic controls.

KEYWORDS

European Alps, flexure, foreland basin, post-orogenesis, Pyrenees, sediment fluxes

1 | INTRODUCTION

Sediment yield from mountain ranges is determined by the geomorphic and climatic characteristics of the system. Catchment size, topographic relief, the amount and intensity of precipitation and glacial activity dominate sediment yield from most ranges (Syvitski & Milliman, 2007). For many settings, these factors are linked to whether the range is tectonically active; for mountain ranges, this is typically when crustal thickening drives rock uplift that sustains steep channel gradients that enable channel incision and consequent collapse of hillslopes (Whipple, 2009). It is therefore to be expected that the rivers that carry the maximum sediment load to the oceans are those that drain the Himalaya such as the Ganga, and the Amazon sourced in the Andes (Syvitski & Saito, 2007). On a global scale, the region with the maximum delivery to the ocean is south-east Asia where most rivers are sourced in active ranges dominated by the Himalaya (Milliman & Farnsworth, 2011).

This is an open access article under the terms of the Creative Commons Attribution License, which permits use, distribution and reproduction in any medium, provided the original work is properly cited.
© 2022 The Authors. *Basin Research* published by International Association of Sedimentologists and European Association of Geoscientists and Engineers and John Wiley & Sons Ltd.

13652117, 0, Downloaded from https://onlinelibrary.wiley.com/doi/10.1111/bre.12727 by Universite De Rennes 1, Wiley Online Library on [08/11/2022]. See the Terms and Conditions (https://onlinelibrary.wiley.com/terms-and-conditions) on Wiley Online Library for rules of use; OA articles are governed by the applicable Creative Commons License

Over geological time, changes in sediment yield from mountain ranges are linked directly to rates of tectonic shortening, thickening and uplift (Sinclair & Allen, 1992; Tucker & Slingerland, 1996). The transfer of orogenically derived sediment to the oceans has been documented using stratigraphic volumes such as on the Atlantic margin east of the Appalachians (Pazzaglia & Brandon, 1996) and the Indus Fan fed by the western Himalaya (Clift, 2006). In these settings, combined climatic and tectonic forcings are considered to control the flux of sediment to the oceans. In locations such as the Rhône fan, which is fed by sediment sourced in the western Alps, sediment volumes have indicated accelerations in the last few millions of years (Kuhlemann et al., 2002) during a time when crustal shortening has slowed. These data from the Alps have been part of a larger database used to argue for global accelerations to continental margins linked to increased erosive capacity for the climate in late Cenozoic times (Molnar, 2004; Peizhen et al., 2001).

Whether changes in sediment yield due to climatic or tectonic forcings are preserved in the oceanic records of sediment accumulation depends largely on the rates of generation of accommodation through subsidence in the foreland basin (Allen et al., 2013). In this respect, foreland basins act to buffer the link between the mountains and the oceans. During the early stages of mountain growth, flexural subsidence generates more than enough space to accommodate the sediment flux from the range, and so deep-water, 'underfilled' conditions dominate in the foreland basin as the orogenically sourced material is trapped in the surrounding troughs. Taiwan (Covey, 1986) and the Eocene and Oligocene history of the North Alpine Foreland Basin (Allen et al., 1991; Sinclair, 1997) are classic examples of underfilled foreland basins.

As mountain ranges and their river catchments expand, so foreland basins become increasingly filled with continental sediments, and river systems flow transverse across the basin (Allen et al., 2013). At this stage, the proportion of orogenically derived sediment that is trapped in the foreland basin determines the flux available to be delivered to continental margins. In the Himalaya, it is thought that only ca. 10% of the total sediment generated in the mountains is trapped in the Gangetic Plains, with the rest being delivered to the Brahmaputra delta (Lupker et al., 2011). Other studies have used cosmogenically induced nuclides such as ^{10}Be to demonstrate rapid bypass of sediment across filled foreland basins such as the Po Basin to the south of the European Alps with little evidence of storage (Wittmann et al., 2016). Similar approaches from the Amazon river using paired ^{26}Al and ^{10}Be indicate rapid transport of Andean-derived fine sediments with no evidence of storage mixed with coarser floodplain sediments that may have been stored since Miocene times (Wittmann et al., 2011). The record of slow recycling for several millions of years for coarser sediment across the Great Plains of Nebraska has also been recorded using the stable cosmogenic nuclide ^{21}Ne (Sinclair et al., 2019). As sediment bypass across foreland basins increases, the connectivity between the mountain range and the oceans also increases, and so tectonic and climatic forcings in the mountain range should be directly recorded in the stratigraphic successions of oceanic sinks; in this scenario, the system is highly reactive as opposed to buffered (Allen, 2008).

In a highly reactive system, it is reasonable to expect that as rates of orogenesis decrease, the sediment flux to the nearby oceans would also decrease. Tucker and van der Beek (2013) introduced a box model to explore the interaction of a coupled mountain range and foreland basin evolving towards post-orogenic decay. They found that the natural state of a decaying system is that the foreland basin undergoes isostatic rock uplift and net erosion which should add to the total sediment accumulation observed in distal depocentres. Bernard et al. (2021) used the same model to explore sediment dispersal from the Pyrenees during the syn- to post-orogenic transition and suggested that sediment flux out of the thrust wedge/foreland basin system may increase at the time at which orogenesis stops. Their analysis indicated that this was caused by the cessation of foreland basin subsidence at a time when the orogenic topography was still generating high sediment yield; the lack of any mechanism to trap the sediment in the basin resulted in accelerated efflux out of the mountain range/foreland basin system. Such mechanisms may explain signals of high sediment flux where the lack of evidence of accelerated tectonic forcing has led

Highlights

- Sediment budget records a cessation of deposition in the foreland basin and acceleration in distal depocentres.
- Numerical modelling shows a signal of sediment flux increased leaving the system at the post-orogenic transition.
- Experiments highlight an optimal erodibility ratio between the range and basin and elastic thickness for the signal.
- First-order control for accelerated sediment flux can be linked to intrinsic processes of an orogenic system.

13652117, 0, Downloaded from https://onlinelibrary.wiley.com/doi/10.1111/bre.12727 by Universite De Rennes 1, Wiley Online Library on [08/11/2022]. See the Terms and Conditions (https://onlinelibrary.wiley.com/terms-and-conditions) on Wiley Online Library for rules of use; OA articles are governed by the applicable Creative Commons License

researchers to the conclusion that climate must be the control (Molnar, 2004; Peizhen et al., 2001). Here, we test this hypothesis of changing sediment yield from mountain belt/foreland basin systems to continental margins during the syn- to post-orogenic transition. We firstly evaluate the evidence from the Pyrenees and the European Alps, both of which have a detailed structural record for the slowing and/or cessation of crustal thickening and a detailed account of changing offshore sediment volumes during the syn- to post-orogenic transition. We then use the coupled tectonic/surface process model Fastscape (Braun & Willett, 2013) to explore the links between changing orogenic erosion rates, flexural subsidence and the external flux to continental margins. Our approach is to balance between a simplification of the model and a reasonable representation of a mountain range and foreland basin system. The main purpose is to understand the main model outputs while approximating the first-order characteristics of the physical processes that govern the system.

For clarity, we define the transition from syn- to post-orogenesis in terms of the topography resulting from the balance between the growth of the range through accretion and crustal thickening versus the erosional efflux to neighbouring basins. This definition equates to the previous terminology used by Jamieson and Beaumont (1988) and Willett and Brandon (2002) where syn-orogenesis corresponds to the 'constructive phase' of a mountain range, whereas post-orogenesis corresponds to the 'destructive phase' of the range. While this definition is focused on the topography of the range, the implications for the foreland basin through flexure of the underlying lithosphere are well understood (Beaumont, 1981; Flemings & Jordan, 1989; Sinclair et al., 1991). Additional processes such as mantle dynamics (e.g. Faccenna et al., 2014) or additional slab loads (e.g. Royden & Karner, 1984) may influence these systems but are independent of the coupling between topography and flexure; their potential influence is discussed for the two case studies.

2 | SEDIMENT ACCUMULATION IN POST-OROGENIC SYSTEMS

Our hypothesis implies the need for accurate records through times of both sediment accumulation in the depositional basins (i.e. foreland basin and surrounding continental margins) and tectonics, in an orogenic system that has evolved under post-orogenic conditions. In the following sections, we analyse two case studies where the syn- to post-orogenic histories are well documented from the Western European Alps and The Northern Pyrenees.

2.1 | The Western European Alps

The European Alps are a doubly vergent orogen resulting from the continental collision between the European Plate and Adriatic microplate. The main phase of crustal thickening of the Alpine thrust wedge occurred between 40 and 17 Ma (Pfiffner, 1986; Schmid et al., 2004). Shortening across the Western Alps continued until at least 5 Ma based on deformation in the Jura and Sub-Alpine Molasse (von Hagke et al., 2014), although Madritsch et al. (2010) also indicate post-Pleistocene tilting of terraces in the Jura that they relate to ongoing compression. GPS data indicate that the western Alps are now experiencing weak extension (Nocquet & Calais, 2003; Sue et al., 2007). Late Miocene to Pliocene slowdown in shortening was associated with some local accelerations in the relative uplift of some of the external massifs indicating that the range was in a state of net contraction (Willett et al., 2006).

Erosion rates averaged over the last few thousands of years using detrital ^{10}Be cosmogenic nuclide concentrations indicate a close correlation with regions of high topography and high rock uplift that may be linked to post-glacial rebound and/or accelerated erosion and rock uplift (Wittmann et al., 2007). Sternai et al. (2019) conclude that post-glacial rebound only accounts for approximately 50% of the present rock uplift and that there has to be a large component linked to sub-lithospheric mantle flow. This is also supported by catchment-wide comparisons of detrital ^{10}Be-derived erosion rates and rock uplift from GPS data across the western Alps (Delunel et al., 2020).

The formation of the North Alpine Foreland Basin (NAFB) during Oligocene and Miocene times results from the flexure of the European continental lithosphere driven by the growth of the Alps (Figure 1). The stratigraphic evolution of the NAFB follows a classical foreland basin succession and comprises two large-scale regressive shallowing- and coarsening-upward megacycles (Homewood et al., 1986; Kuhlemann & Kempf, 2002). Traditionally, the NAFB is divided into four depositional groups: the Lower Marine Molasse and Lower Freshwater Molasse groups that constitute the first megacycle; the Upper Marine Molasse and Upper Freshwater Molasse which constitute the second megacycle. However, the earliest foreland basin fill also includes the North Helvetic Flysch that extended the marine history of the basin from at least 42 Ma to 29 Ma. The Lower Freshwater Molasse (29–22 Ma) record the filling of the basin with the development of large alluvial fans up to 3 km thick that flowed transverse to the mountain front, but then deflected to an easterly axial flow in their distal parts (Schlunegger et al., 1997). The Upper Marine Molasse marks a return to shallow marine conditions with a tidal seaway linking to the

13652117, 0, Downloaded from https://onlinelibrary.wiley.com/doi/10.1111/bre.12727 by Universite De Rennes 1, Wiley Online Library on [08/11/2022]. See the Terms and Conditions (https://onlinelibrary.wiley.com/terms-and-conditions) on Wiley Online Library for rules of use; OA articles are governed by the applicable Creative Commons License

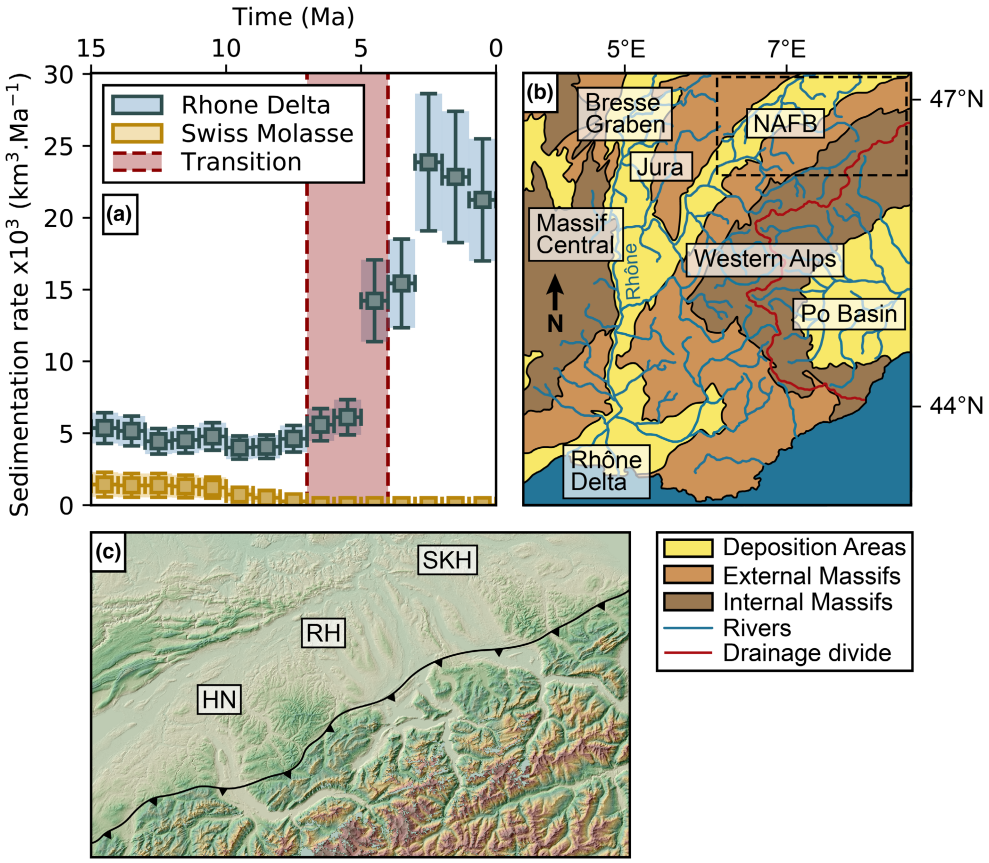

FIGURE 1 Source to sink system of the Western European Alps. (a) Sediment budget in the North Alpine Foreland Basin (NAFB) and Rhône Delta since 15 Ma from Kuhlemann et al. (2001). Yellow and blue squares indicate the rate of sediment accumulation for the North Alpine Foreland Basin and the Rhône Delta depocentres respectively. Red-shaded bar corresponds to the estimated timing of the post-orogenic transition. (b) Geographic map of the fluvial network of the Western Alps. Blue lines correspond to the main rivers. The red line corresponds to the main drainage divide of the European Alps. (c) Elevation map of the Western European Alps and southern NAFB draped on a hillshade map. Both maps are from the SRTM digital elevation model with a resolution of 30 m (https://earthexplorer.usgs.gov/). HN, Honegg-Napf fan; RH, Rigi-Höhronen fan; SKH, Speer-Kronberg-Hörnli fan.

Mediterranean along the present Rhône valley (Martel et al., 1994). The Upper Freshwater Molasse records a filling of the basin around 16 Ma with alluvial fans that feed a system that flowed southwestward (Kuhlemann & Kempf, 2002). Between approximately 11 and 5 Ma, the North Alpine Foreland Basin of Switzerland ceased being a site of sediment accumulation and switched to being actively eroded as recorded by thermochronological data from wells in the basin that record active exhumation of the basin starting around 5 Ma (Cederbom et al., 2004, 2011). Some of the erosion of the foreland basin is likely to have also been associated with drainage reorganisation (Schlunegger & Mosar, 2011; Winterberg & Willett, 2019). The modern topography of the 'Molasse Basin' is incised and erosive as shown by channel incisions along paleo-fans (i.e. Honegg-Napf, Rigi-Höhronen fan and Speer-Kronberg-Hörnli fans) (Figure 1c).

Based on extensive sediment volume measurements, Kuhlemann et al. (2001) demonstrate that sediment accumulation rates during orogenesis remained fairly steady (Figure 1a) with variations determined by processes such as slab break-off driving the underfilled to filled transition (Sinclair, 1997) and underplating driving the accelerated exhumation of the external Massifs. Post-orogenesis forced the isostatic rebound and exhumation of the NAFB (see above). In contrast, the sediment accumulation in the more distal depocentres such as the Po Basin, Rhône Delta and the North Sea experienced an accelerated influx of sediment from around 5 Ma (Figure 1a) (Kuhlemann et al., 2001). Although the use of sediment volume data in this way has been challenged based on the increased preservation bias towards younger successions in the stratigraphic record (Sadler, 1981; Willenbring & Jerolmack, 2016). Given the post-orogenic context of this accelerated sediment flux, it has been widely interpreted as a result of changes to the erosional capacity of the late Cenozoic climate systems (Cederbom et al., 2004; Kuhlemann et al., 2001; Molnar, 2004; Willett, 2010) or to slab detachment and surface uplift (Baran et al., 2014; Fox et al., 2015).

13652117, 0, Downloaded from https://onlinelibrary.wiley.com/doi/10.1111/bre.12727 by Universite De Rennes 1, Wiley Online Library on [08/11/2022]. See the Terms and Conditions (https://onlinelibrary.wiley.com/terms-and-conditions) on Wiley Online Library for rules of use; OA articles are governed by the applicable Creative Commons License

2.2 | The Northern Pyrenees

The Pyrenean mountain belt is a doubly vergent collisional orogen which results from convergence between the Iberian microplate and the European plate from late Cretaceous time (i.e. 84 Ma) to early Miocene time (i.e. ca. 20 Ma) (Roest & Srivastava, 1991). The main phase of convergence and development of the Pyrenean thrust wedges occurred during the Eocene and Early Oligocene while the cessation of convergence has been dated at around Late Oligocene to early Miocene time. The dating of the transition to post-orogenesis is based on a range of data. Cooling records from different isotopic systems in the Central Pyrenees (Fitzgerald et al., 1999; Gibson et al., 2007; Morris et al., 1998; Sinclair et al., 2005) suggest that exhumation slowed down significantly after 30–25 Ma with the latest cooling in the Barruera massif located in the southern pro-wedge (Gibson et al., 2007; Sinclair et al., 2005). Young cooling ages record local late exhumation in the Pyrenees (Fillon et al., 2021; Gibson et al., 2007; Jolivet et al., 2007). The end of deformation determined by magnetostratigraphy on growth strata attached to the front of the Pyrenean thrust belt occurred during the upper Oligocene time around 25 Ma (Meigs et al., 1996). Using an inverse modelling of the flexural subsidence through time of the Pyrenean foreland basins, Curry et al. (Curry et al., 2019) inferred the topographic evolution of the Pyrenees and estimated maximum topography during Oligocene time followed by minor topographic decay during the Miocene.

The Aquitaine Basin represents the retro-foreland basin of the Pyrenees that records the flexural response to topographic and subsurface loads (Brunet, 1986; Desegaulx et al., 1990; Rougier et al., 2016) (Figure 2). As is typical of retro-foreland basins, the Aquitaine Basin preserves the full stratigraphic record of the Pyrenean growth (Naylor & Sinclair, 2008). The pre-orogenic stratigraphy starts with red sandstones, evaporites and shallow marine deposits deposited during Triassic rifting (Rougier et al., 2016). Sedimentation during Jurassic and Cretaceous times was dominated by marine carbonate, marl and dolomite deposition (Biteau et al., 2006). During the principal rifting phase from Aptian to early Cenomanian, sedimentation comprised deep marine clastics (Black Flysch group) and rim carbonates (Pierrelys group) (Debroas, 1990). Syn-orogenic sedimentation start during the Upper Cretaceous and Palaeocene periods and accumulated mainly under marine conditions with deposition of the Grey and Black Flysch, Petite Pyrenees, Aude Valley, Coustouge and Rieuback Groups (Ford et al., 2016; Rougier et al., 2016). During the Late Ypresian time, sedimentation became predominantly continental in the eastern basin (Bourrouilh et al., 1995; Ford et al., 2016). The marine-continental transition migrates westward with the deposition of the Upper and Lower Carcassonne Group during Oligocene and Early Miocene times. As a part of this process, Aquitanian and lower Burdigalian stratigraphy (ca. 23–19 Ma) records an unconformity associated with sediment bypass to the east; this is overlain by a few 100 m of upper Burdigalian to Quaternary proximal alluvial fan, braided fluvial and shallow marine deposits (Gardère et al., 2002; Ortiz et al., 2020). Conglomeratic deposits of the post-orogenic upper Carcassone Group dated at ca. 12 Ma drape the margins of the north Pyrenean thrust wedge up to elevations of ca. 600 m (Bernard et al., 2021). These deposits correspond to the development of large alluvial fans that draped the syn-orogenic structures of the North Pyrenean thrust wedges (Figure 2c). They represent a period of accumulation of post-orogenic continental sediment driven by a reduction in accommodation space related to the slowdown of subsidence in the basin. Proximal parts of the Adour, Lannemezan and Salat fans are located at high elevations (e.g. ca. 400–600 m). The modern morphology of the Aquitaine basin is dominated by erosion highlighted by channel incisions along the fans and up to the mountain front (Figure 2c).

The volume of sediment preserved during the Cenozoic period has been determined by Sinclair et al. (2005) from several wells in the Aquitaine Basin. Sedimentation rates were high (0.05 mm/year) during the Palaeocene-Lower Eocene and Upper Eocene periods. From Oligocene to Miocene times, sediment accumulation rates in the Aquitaine Basin decreased to around 0.02 mm/year. However, the data set used in this study could not differentiate the Oligocene and Miocene periods, that is the late syn- to post-orogenic transition. In a more recent study, Ortiz et al. (2020) combined seismic lines and deep good data from the Aquitaine Basin and the deep Bay of Biscay in order to produce isopach maps for different periods of times. Sediment accumulation in the Aquitaine foreland basin is active during the syn-orogenic period of the Pyrenees (i.e. ca. 66–ca. 23 Ma) with slightly more important deposition during the Oligocene period (Figure 2a) (Ortiz et al., 2022). The Oligocene–Miocene transition (i.e. 23 Ma) is marked by a drastic reduction in sedimentation rate in the foreland basin. Since Miocene time, the basin records very limited amount of sediment deposition. Sediment accumulation in the Bay of Biscay remains very low during the Palaeocene and Eocene periods (Figure 2a). Two phases of acceleration in sediment accumulation are recorded around Oligocene time and late Miocene time.

13652117, 0, Downloaded from https://onlinelibrary.wiley.com/doi/10.1111/bre.12727 by Universite De Rennes 1, Wiley Online Library on [08/11/2022]. See the Terms and Conditions (https://onlinelibrary.wiley.com/terms-and-conditions) on Wiley Online Library for rules of use; OA articles are governed by the applicable Creative Commons License

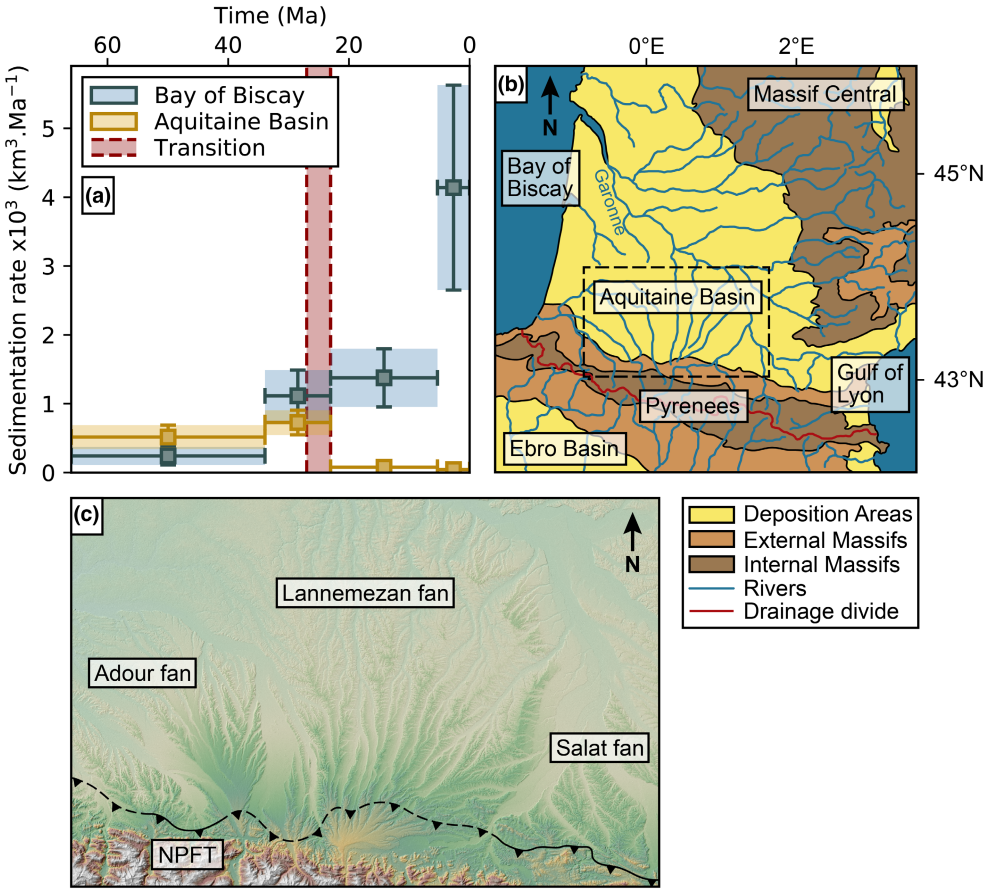

FIGURE 2 Source to sink system of the northern Pyrenees. (a) Sediment budget in the Aquitaine Basin and Bay of Biscay during Cenozoic time from Ortiz et al. (2022)). Yellow and blue squares indicate the rate of sediment accumulation for the Aquitaine Basin and the Bay of Biscay depocentres respectively. Red-shaded bar corresponds to the estimated timing for the post-orogenic transition. (b) Geographic map of the Pyrenees, Aquitaine Basin and Bay of Biscay system. Blue lines correspond to the main rivers. The red line corresponds to the drainage divide of the Pyrenees. A black dash rectangle indicates the location of the hillshade map. (c) Elevation map of the central northern Pyrenees and Aquitaine Basin draped on a hillshade map. Both maps are from the SRTM digital elevation model with a resolution of 30 m (https://earthexplorer.usgs.gov/). NPFT, North Pyrenean Frontal Thrust.

3 | METHODS

3.1 | Model algorithm

We have shown that for both the Western European Alps and the Northern Pyrenees, there appears to have been a first-order trend between the timing of post-orogenesis, the cessation of sediment deposition in foreland basins and the acceleration of sediment discharge to distal depocentres. Here, we explore the link between crustal thickening, topographic growth, foreland basin flexure and sediment flux in order to evaluate the impact on sediment dispersal during the onset of post-orogenic decay of a mountain belt/foreland basin system. Our orogenic system (i.e. mountain range and foreland basin) is modelled using the two-dimensional landscape evolution model Fastscape (Braun & Willett, 2013), available through the Xarray-Simlab package (Bovy, 2020). We take full advantage of model equations that simulate erosion, transport and deposition in both continental and marine domains (Yuan, Braun, Guerit, Simon et al., 2019). Continental erosion is controlled by river channel incision and hillslope processes with the stream power model and linear diffusion law respectively:

$$E = K_f A^m S^n + K_c \nabla^2 h, \quad (1)$$

where E is erosion rate (m/year), A is drainage area (m^2), S is the slope and is dimensionless, m and n are area and slope exponents respectively, h is the elevation (m), K_f is the erodibility coefficient (m^{1-2m}/year) and K_c is a transport coefficient (m^2/year). Transport and sediment deposition in the continental domain are included in the model with the following condition:

$$D = \frac{G}{A}\int_A \left(U - \frac{\mathrm{d}h}{\mathrm{d}t}\right)\mathrm{d}A, \quad (2)$$

13652117, 0, Downloaded from https://onlinelibrary.wiley.com/doi/10.1111/bre.12727 by Universite De Rennes 1, Wiley Online Library on [08/11/2022]. See the Terms and Conditions (https://onlinelibrary.wiley.com/terms-and-conditions) on Wiley Online Library for rules of use; OA articles are governed by the applicable Creative Commons License

where D is the deposition rate (m/year) and G is a coefficient for deposition. The coefficient for deposition (G) is related to the size of sediment and the settling velocity by the mathematical formula $G = d^* v_s / p_0$, where d^* is the ratio between the sediment concentration near the riverbed interface and the average concentration over the water column, v_s is the net settling velocity of sediment grains and p_0 is the mean precipitation. In this model, the stream power law formulation works with fluxes, therefore, we do not consider the effect of grain size (Yuan, Braun, Guerit, Rouby et al., 2019). In the marine domain, sediment transport and deposition are simulated through a diffusion equation:

$$\frac{\mathrm{d}h}{\mathrm{d}t} = K_n \nabla^2 h + Q_s, \tag{3}$$

where t is time (year), K_n is the marine sediment transport coefficient (m^2/year) and Q_s is the sediment flux (m/year) coming from the continental part of the model.

The Fastscape model also incorporates flexural isostasy and considers any change in surface topography as a load proportional to surface density on a thin continuous elastic plate of uniform properties (Braun et al., 2014). The surface deflection added to the surface topography is obtained with a spectral method by solving the bi-harmonic equation:

$$D\left(\omega_{xxxx} + 2\omega_{xxyy} + \omega_{yyyy}\right) = \left(\rho_a - \rho_s\right)\omega + \rho_s g\left(h - h_0\right) \tag{4}$$

with

$$D = \frac{Y_m T_e^3}{12\left(1 - \nu^2\right)}, \tag{5}$$

where ω is the deflection, ρ_a is the density (kg/m^3) of the underlying asthenosphere, ρ_s is the density (kg/m^3) of the material being eroded, g is the gravitational acceleration (m/s^2), h_0 and h correspond to the initial elevation and the elevation (m) (i.e. modified after erosion, uplift or deposition) respectively, Y_m is the young modulus, T_e is the effective elastic thickness (m) and ν is the Poisson's ratio. D defines the flexural rigidity of the plate and hence the wavelength of flexure. Boundaries in the model can be defined with different conditions: (1) open boundary, (2) close boundary and (3) periodic boundary.

3.2 | Model setup

The model comprises a total area of 400 km in length and 400 km in width with a horizontal and vertical number of grid nodes of 200 in order to keep a uniform spatial resolution of 2 km (Figures 3a and 4a). The model comprises

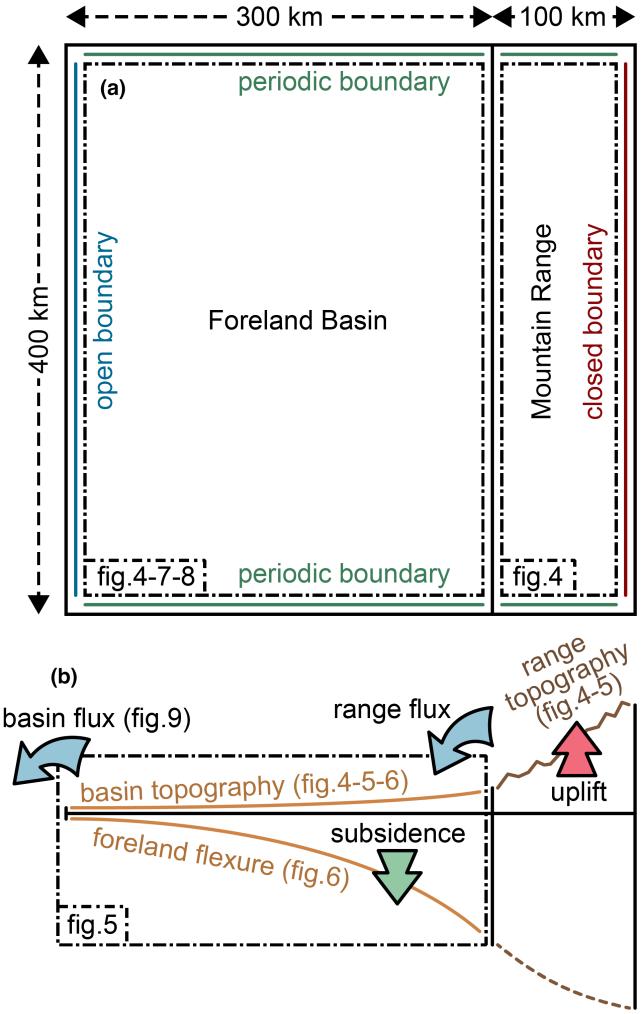

FIGURE 3 Model configuration simulating an orogenic system. (a) Planar view of the model with dimensions of the different areas and the boundary conditions. (b) Cross-section view of the model highlighting dynamics of the model. Note that during post-orogenesis, uplift is no longer active and the basin flexure evolves under rebound condition (i.e. green arrow is therefore reversed) as the range topography decrease.

two distinct (Figures 3b and 4c) areas that correspond to (1) the mountain range on the right of the model with a width of 100 km and (2) the foreland basin on the left side of the model with a width of 300 km. Model areas are initialised at the beginning of the experiment and cannot change through time. The boundary between these model domains is vertical and approximates the deformation front.

The model evolves over a duration of 140 Myr with a time resolution of 5×10^4 years, giving a total number of 2800 timesteps. An uplift rate of 1.5 mm/year is imposed on the mountain range from the start of the simulation to 120 Myr (i.e. from 0 to 120 Myr, the system evolves under syn-orogenic conditions). From 120 Myr to the end of the simulation, the uplift rate is set to 0 mm/year (i.e. from

13652117, 0, Downloaded from https://onlinelibrary.wiley.com/doi/10.1111/bre.12727 by Universite De Rennes 1, Wiley Online Library on [08/11/2022]. See the Terms and Conditions (https://onlinelibrary.wiley.com/terms-and-conditions) on Wiley Online Library for rules of use; OA articles are governed by the applicable Creative Commons License

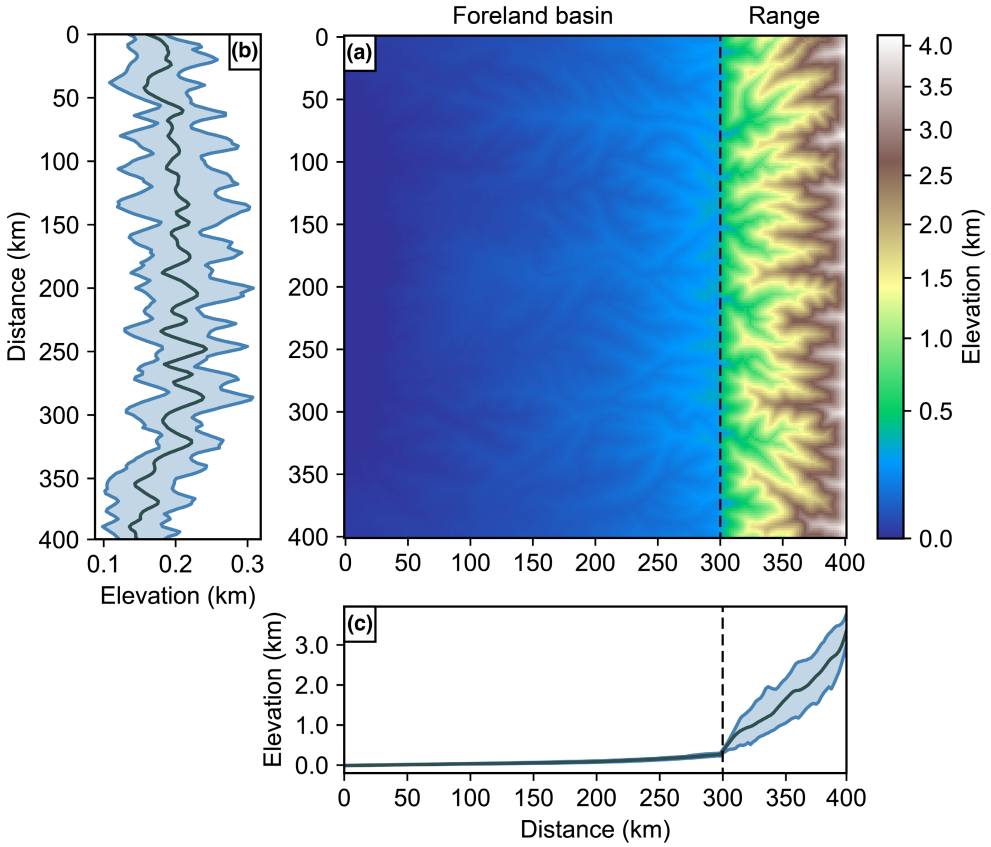

FIGURE 4 Topography of the numerical model at 127 Ma (timing for the maximum mean elevation of the foreland basin during post-orogenesis. (a) Topography of the foreland basin and range. (b) Transversal swath profile of the proximal part of the foreland basin showing the mean elevation (dark blue line) and the 5th and 95th percentile (light blue lines). (c) Longitudinal swath profile of the foreland basin and range showing the mean elevation (dark blue line) and the 5th and 95th percentile (light blue lines).

140 to 120 Myr, the system evolves under post-orogenic conditions).

We initially set a base model and then explored the sensitivity to variations in these values. We set a spatially uniform erodibility coefficient of 1×10^{-6} in the mountain range area. Although erodibility should highlight some variability related to different lithologies, our range coefficient is in the range of values deduced for rocks found in mountain ranges (Gallen, 2018; Zondervan et al., 2020). We choose an erodibility coefficient of 5×10^{-6} in the foreland basin in order to replicate weaker rocks compare to the mountain range. We define a deposition coefficient of 1 as it is in good agreement with estimates from the natural sedimentary system (Guerit et al., 2019). The area (m) and slope (n) exponents are 0.44 and 1.0, respectively, and give a concavity index (θ) of 0.44 which falls within the range of concavities (i.e. 0.35–0.6) found by studies that have analysed the relationship between drainage area and local slope (Kirby & Whipple, 2012; Whipple & Tucker, 1999).

The mountain range and foreland basin are coupled by flexure with an asthenosphere and lithosphere density of 3300 and 2700 kg m^3, respectively, and a lithosphere elastic thickness of 22 km based on values for young Tethyan mountain ranges such as the Pyrenees and Alps (Karner & Watts, 1983; Rougier et al., 2016). Young modulus and Poisson's ratio properties are set by default to 1×10^{11} and 0.25 respectively. The left boundary of the model is set as open and allows sediment flux to leave the system (i.e. the foreland basin). The right boundary status is closed and should correspond to the drainage divide of the thrust wedge. Top and lower boundaries are periodic in order to simulate a continuous orogenic system. The parameters of the model are presented in Table 1.

4 | RESULTS

4.1 | Orogenic development

The topographic evolution of the mountain range is characterised by an increase of the mean elevation during the simulated syn-orogenic period (i.e. 0–120 Myr when uplift is active) (Figure 5a). Elevation changes of the range become progressively limited through the syn-orogenic period as the system reaches steady-state conditions (i.e. erosion counteracts uplift). At the end of syn-orogenesis,

13652117, 0, Downloaded from https://onlinelibrary.wiley.com/doi/10.1111/bre.12727 by Universite De Rennes 1, Wiley Online Library on [08/11/2022]. See the Terms and Conditions (https://onlinelibrary.wiley.com/terms-and-conditions) on Wiley Online Library for rules of use; OA articles are governed by the applicable Creative Commons License

the mean elevation of the range reaches about 2 km with maximum elevations at ca. 4.5 km. During the post-orogenic period (i.e. 120–140 Myr when uplift is no longer active), the topography of the range decreases through time with an inverse exponential shape (Figure 5).

TABLE 1 Parameters for the simulation

Notation	Definition	Values	Unit
x	Horizontal dimension	400	km
y	Horizontal dimension	400	km
Δx	Cell size	2	km
Δy	Cell size	2	km
t	Time	140	Myr
Δt	Incremental time	5×10^{4}	yr
U	Uplift rate	1.5	mm/yr
K_m	Range erodibility coefficient	1×10^{-6}	m^{1-2m}/yr
K_b	Basin erodibility coefficient	5×10^{-6}	m^{1-2m}/yr
G	Deposition coefficient	1	–
m	Area exponent	0.44	–
n	Slope exponent	1	–
ρ_a	Asthenosphere density	3300	kg/m^3
ρ_s	Lithosphere density	2700	kg/m^3
T_e	Lithosphere elastic thickness	22	km
Y_m	Young modulus	1×10^{11}	–
ν	Poisson's ratio	0.25	–

The foreland basin shows a more complex topographic evolution through its lifecycle (Figure 5b). Mean elevation remains negative during the early part of the syn-orogenic period simulating the initial underfilled stage of foreland basin development (e.g. Covey, 1986). At about 15 Myr, mean elevations become positive and increase through time as the basin fills. Similar to the topography of the mountain range, the rate of increase of the foreland basin mean elevation decreases towards the end of syn-orogenesis as the system reaches a near steady-state topographic condition. The transition to post-orogenesis is characterised in the foreland basin by an increase in the basin's elevation (Figure 5b,d). The basin's mean elevation reaches a maximum of about 50–70 m at around 127 Myr in the experiment; that is ca. 7 million years after cessation of tectonically driven rock uplift in the thrust wedge. Following the general increase, the mean elevation of the basin shows a continued and limited decrease until the end of the simulation.

The topographic long profile of the foreland basin highlights the increase in elevation following the post-orogenic transition (Figure 6). Elevation change is particularly noticeable in the proximal part of the basin (Figure 6a–c) from 120 to 124 Myr. Maximum elevations observed at the mountain front go from ca. 190 m at 120 Myr to ca. 265 m at 128 Myr with the formation of important fans (Figure 4a). As observed in the mean elevation of the basin (Figure 5b),

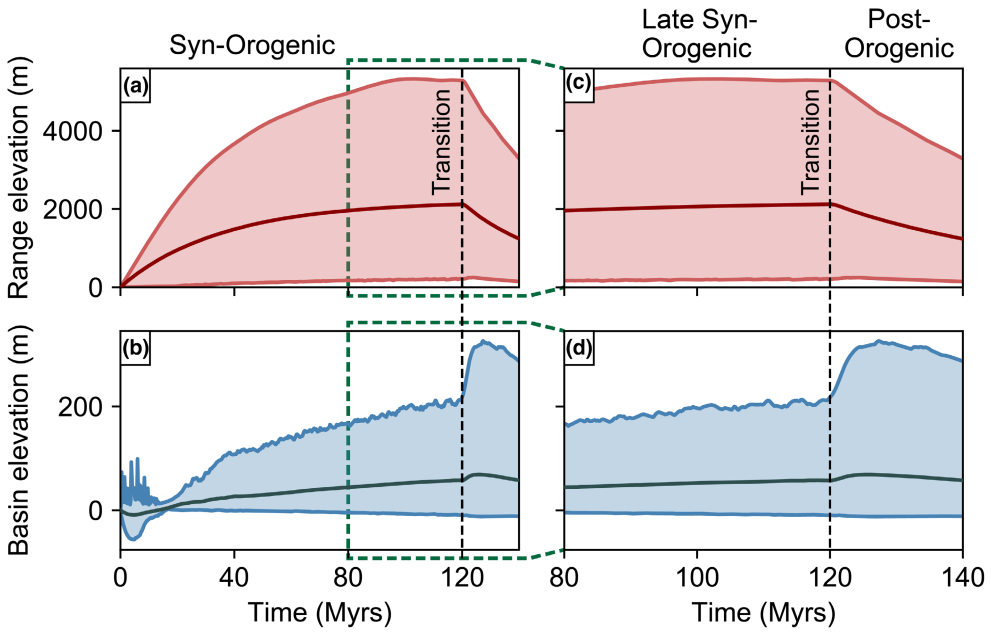

FIGURE 5 Topographic evolution of a simulated orogenic system. (a) Elevation of the mountain range. The dark red line corresponds to the mean elevation. Light red lines correspond to the maximum and minimum elevations. (b) Close-up of syn- to post-orogenic transition (c) elevation of the foreland basin. The dark blue line corresponds to the mean elevation. Light blue lines correspond to the maximum and minimum elevation. Dash black lines correspond to the syn- to post-orogenic transition. (d) Close-up of syn- to post-orogenic transition.

13652117, 0, Downloaded from https://onlinelibrary.wiley.com/doi/10.1111/bre.12727 by Universite De Rennes 1, Wiley Online Library on [08/11/2022]. See the Terms and Conditions (https://onlinelibrary.wiley.com/terms-and-conditions) on Wiley Online Library for rules of use; OA articles are governed by the applicable Creative Commons License

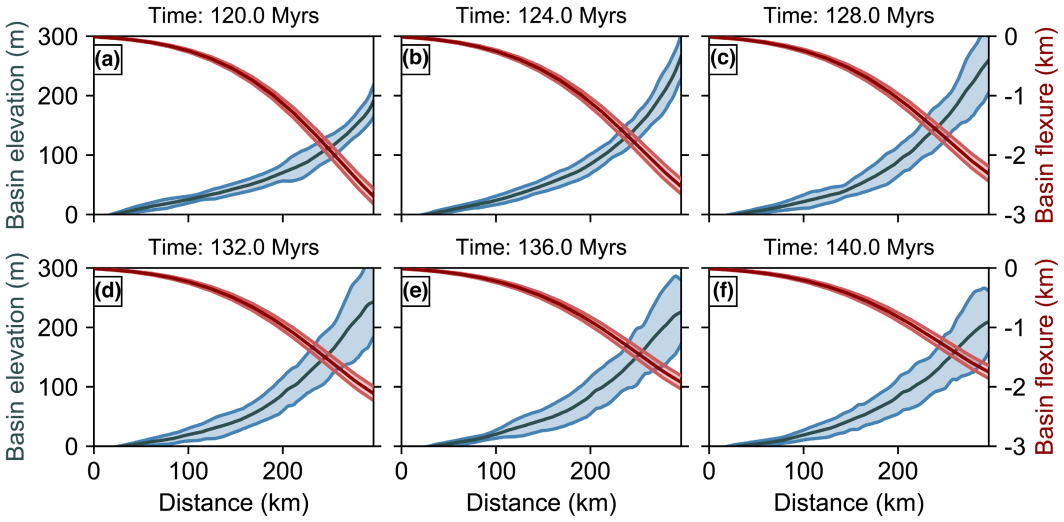

FIGURE 6 Longitudinal profile of the average surface elevation (blue) and flexural basement (red) along the foreland basin at different time steps of post-orogenesis (i.e. 120, 124, 128, 132, 136 and 140 Myr). Dark blue and light blue lines correspond to the mean and 1σ uncertainties of the foreland basin elevation respectively. Dark red and light red lines correspond to the mean and 1σ uncertainties of the foreland basin basement respectively. Basin flexure decreases through time, and basin elevation increases from 120 to 128 Myr (a, b and c) and decreases from 128 to 140 Myr (d, e and f).

elevation along the basin long profile decreases after 128 Myr. Compared to the early post-orogenic increase, the topographic decay is relatively limited with elevations going from ca. 290 m to ca. 205 m at the end of the simulation. The long profile of basement flexure beneath the foreland basin during the post-orogenic period is characterised by a general reduction in depth. The depth of the flexed basement at the front range decreases from ca. 2.75 km at 120 Myr to ca. 1.8 km at 60 Myr as the flexural profile rebounds upward (Figure 6a,f). The morphology of the modelled foreland basin during the post-orogenic phase (Figure 4a) presents important similarity with the modern Aquitaine and 'molasse' basin (Figures 1c and 2c) with the development of fans at high elevation in the proximal part of the basin (Figure 4b) and channel incision all along the basin. To sum up the post-orogenic topographic evolution, the mountain range is characterised by a long-term decay and the foreland basin initially increases in elevation followed by a decrease while the entire system is subject to rebound of the flexural basement.

Following the syn- to post-orogenic transition, the foreland basin still evolves under a combination of erosion and deposition fluctuating through time (Figure 7a–d). The proximal part of the basin progressively switches from being dominated by deposition to erosion characterised by channel incision near the mountain front (Figure 7e–l). This process change is synchronous with the flexural rebound occurring mainly in the proximal part of the basin as observed from the flexure long profile record (Figure 6). After about 128 Myr, deposition becomes very limited and the entire basin evolves under erosional conditions (Figure 8e–l). The dynamics of the mountain range and foreland basin control the amount of sediment leaving the system (Figure 9). During syn-orogenesis, sediment flux leaving the system starts around 20 Myr when the foreland basin becomes filled and starts to bypass, and this then increases through time proportional to the range elevation. An important increase in sediment outflux from the mountain range/foreland basin system is observed at the transition to post-orogenesis, associated with the switch from deposition to erosion in the foreland basin (Figure 6). The sediment outflux increases from ca. 10 to ca. 12×10^8 km^3/Myr and lasts until about 126 Myr and is followed by a steady decrease (Figure 9). This 20% increase in the sediment outflux will be transferred to the next downstream depocentre, which in most instances is the continental margin.

4.2 | Sensitivity analyses

The increase of sediment flux leaving the foreland basin at the post-orogenic transition is dependent on a range of model parameters. First, we test the initial rock uplift rate. Second, we test the erodibility coefficient ratio: K_b / K_m, where K_b is the erodibility coefficient of the basin and K_m is the erodibility coefficient of the range. Finally, we test the effect of the lithosphere elastic thickness. By default, we use values cited in the model setup section (i.e. uplift rate: 1.5 mm/year, basin erodibility: 5×10^{-6}, range erodibility: 1×10^{-6} and elastic thickness: 22 km) as a reference model. Here, we focus on the absolute increase in

13652117, 0, Downloaded from https://onlinelibrary.wiley.com/doi/10.1111/bre.12727 by Universite De Rennes 1, Wiley Online Library on [08/11/2022]. See the Terms and Conditions (https://onlinelibrary.wiley.com/terms-and-conditions) on Wiley Online Library for rules of use; OA articles are governed by the applicable Creative Commons License

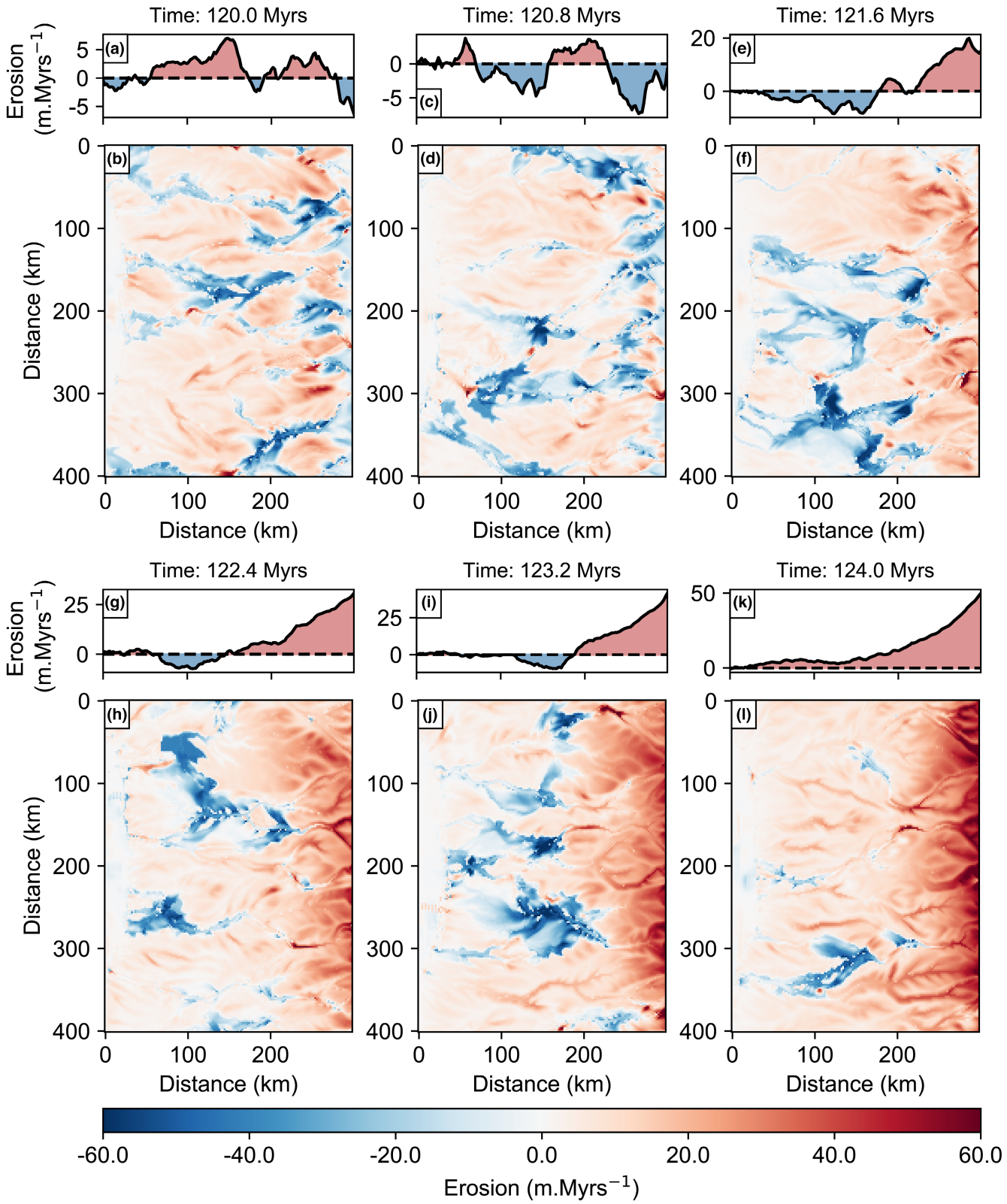

FIGURE 7 Pattern of erosion and deposition in the foreland basin at different time steps during post-orogenesis (i.e. 120.0, 120.8, 121.6, 122.4, 123.2 and 124 Myr). Each image represents the cumulative erosion and deposition over the 50,000-year time interval. Blue and red colours indicate the area of deposition and erosion respectively. (a, c, e, g, i and k) Transversal mean erosion or deposition along the foreland basin. (b, d, f, h, j and l) Plan view of the foreland basin. The left and right borders represent the surrounding continental margin and the mountain front respectively. During early post-orogenesis (a–d), the basin is dominated by a mix between erosion and deposition. Through the simulation, the proximal part of the basin switches towards domination of erosion (e–l).

13652117, 0, Downloaded from https://onlinelibrary.wiley.com/doi/10.1111/bre.12727 by Universite De Rennes 1, Wiley Online Library on [08/11/2022]. See the Terms and Conditions (https://onlinelibrary.wiley.com/terms-and-conditions) on Wiley Online Library for rules of use; OA articles are governed by the applicable Creative Commons License

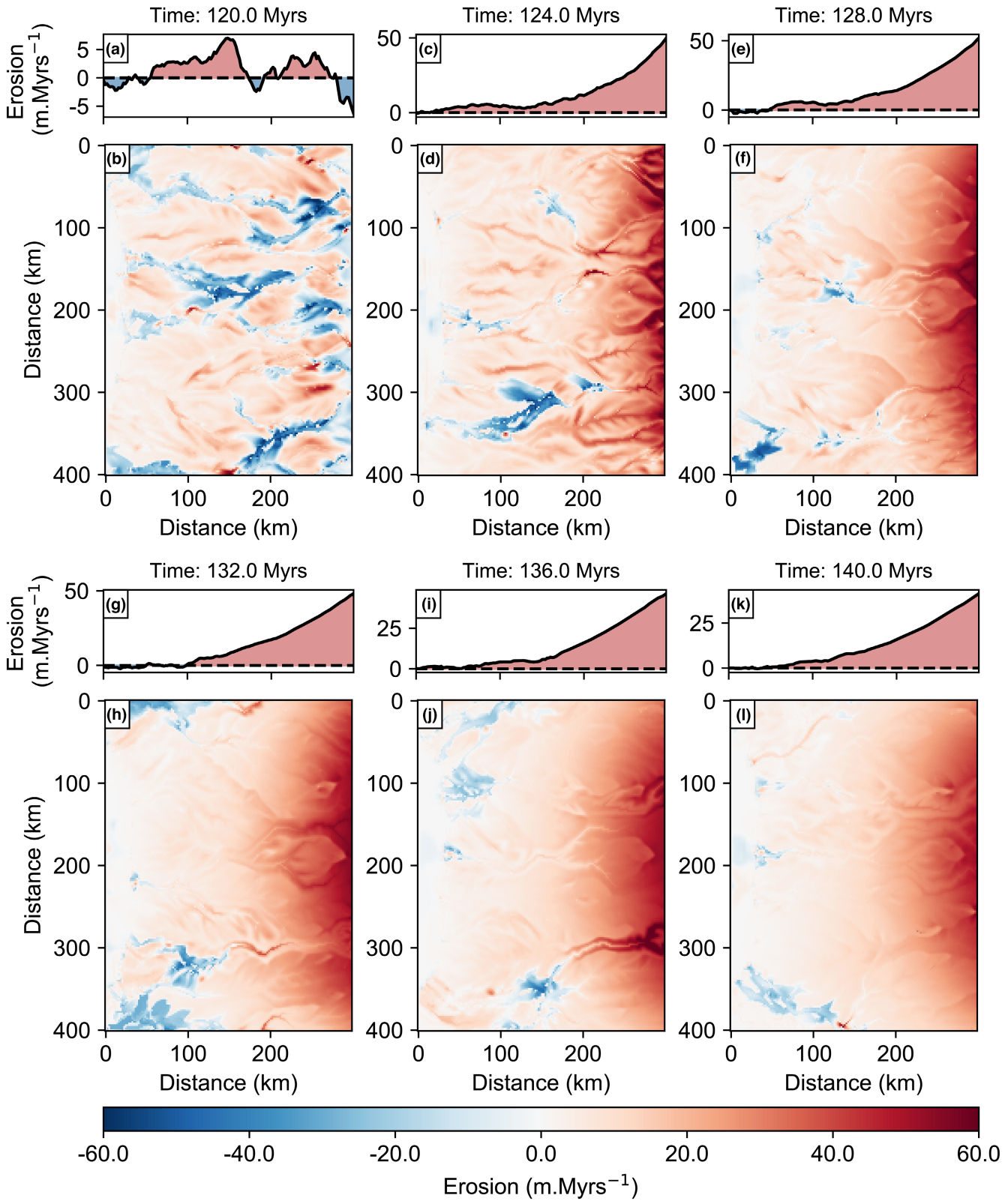

FIGURE 8 Pattern of erosion and deposition in the foreland basin at different time steps during post-orogenesis (i.e. 120, 124, 128, 132, 136 and 140 Myr). Each image represents the cumulative erosion and deposition over the 50,000-year time interval. Blue and red colours indicate area of deposition and erosion respectively. (a, c, e, g, i and k) Transversal erosion or deposition averaged north–south along the foreland basin. (b, d, f, h, j and l) Plan view of the foreland basin. The left and right borders of the view correspond to the limits of the foreland basin with the surrounding continental margin and with the mountain front respectively. During early post-orogenesis (a–d), the foreland basin evolves mainly a mix of erosion and deposition conditions. In contrast, during late post-orogenesis (e–l), the foreland basin evolves mainly under erosion conditions. Note the channel incision into the proximal uplifting foreland basin.

13652117, 0, Downloaded from https://onlinelibrary.wiley.com/doi/10.1111/bre.12727 by Universite De Rennes 1, Wiley Online Library on [08/11/2022]. See the Terms and Conditions (https://onlinelibrary.wiley.com/terms-and-conditions) on Wiley Online Library for rules of use; OA articles are governed by the applicable Creative Commons License

sediment outflux following the post-orogenic transition (Figure 10). The absolute increase corresponds to the difference between the sediment flux measured at 120 Ma and the maximum sediment flux measured during the post-orogenic period.

4.2.1 | Rock uplift rate

Sensitivity to the initial rock uplift rate in the range shows that there is a linear relationship between this parameter and the increase of sediment outflux following the post-orogenic transition (Figure 10a). For higher rock uplift rates, the increase in sediment outflux is proportionally greater. A higher rock uplift rate implies more growth of the range and, therefore, higher flexure of the lithosphere. Consequently, when uplift ceases and the topography of the range is reduced, the degree of isostatic rebound in the foreland basin is also proportionally more important. Higher rebound is recorded by the basin surface uplift and erosion rates leading to higher increases of sediment outflux (Figure 10a). Because of the stream power model, it is important to note the relationship between the uplift (U) and the erodibility (K_m) which affect the range. There is a scaling between the uplift and the range erodibility meaning that an increase in the range erodibility can compensate for an increase in the uplift. Therefore, the result of this section can also be applied to any change in the range erodibility.

4.2.2 | Erodibility coefficient ratio (K_b / K_m)

This parameter controls the efficiency of erosion between the basin and range. Erodibility (i.e. K_f in the stream power law) refers to the efficiency of erosion and should reflect variation in lithology or climate (i.e. higher erodibility means weaker rock types or higher precipitation). A negative ratio means that erodibility is higher in the range than in the basin and vice versa. The erodibility ratio has to be larger than or equal to 3 in order to observe a notable increase in sediment flux following the post-orogenic transition (Figure 10b). For a basin with a low erodibility (i.e. lower erodibility ratio), erosion of the foreland basin during the post-orogenic isostatic rebound is limited. In this scenario, the signal of sediment flux leaving the system during post-orogenesis is dominated by the erosion of the range in contrast to a limited contribution from the erosion of the basin. Given most foreland basins are characterised by unconsolidated sands with high erodibility, this scenario is only likely to occur in extremely arid settings where sediment delivered from the range simply aggrades over the basin. Similarly, a higher range erodibility (i.e. lower erodibility ratio) results in higher erosion of the range and leads to more sediment yield from the range. In this case, the signal from the uplifted and eroded basin is therefore overridden by the range sediment outflux. We can note also that a higher range erodibility limits the growth of the range and the flexure of the lithosphere. Consequently, the amount of isostatic rebound and erosion in the basin is less important and limits the increase of sediment outflux at the post-orogenic transition. It demonstrates that in order to observe an increase in the contribution of material eroded from the basin, the ability for surface processes dominated by rivers in the basin, have to be high relative to the range. For most foreland basins, it is normal to expect the recently deposited sediment to be more easily eroded by fluvial processes than the bedrock exhumed in the mountain catchments.

4.2.3 | Lithospheric thickness

For a model with a basin erodibility of 5×10^{-6} and a range erodibility of 1×10^{-6}, the maximum increase in

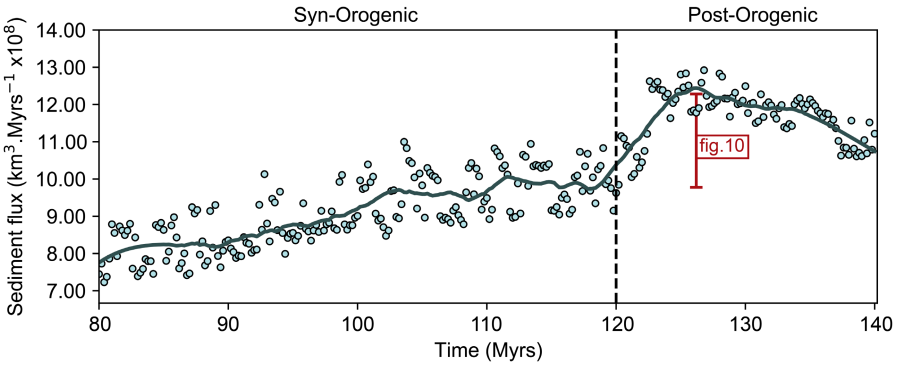

FIGURE 9 Evolution of the sediments leaving the model system (left border for Figures 4, 6 and 7) during syn- and post-orogenesis which corresponds to the sediments delivered to the surrounding continental margins. Blue dots correspond to the mean sediment flux at the left border of the foreland basin at each time step, and the line represents the running mean. The red scale shows the sediment flux measurement used for the sensitivity analyses in Figure 10.

13652117, 0, Downloaded from https://onlinelibrary.wiley.com/doi/10.1111/bre.12727 by Universite De Rennes 1, Wiley Online Library on [08/11/2022]. See the Terms and Conditions (https://onlinelibrary.wiley.com/terms-and-conditions) on Wiley Online Library for rules of use; OA articles are governed by the applicable Creative Commons License

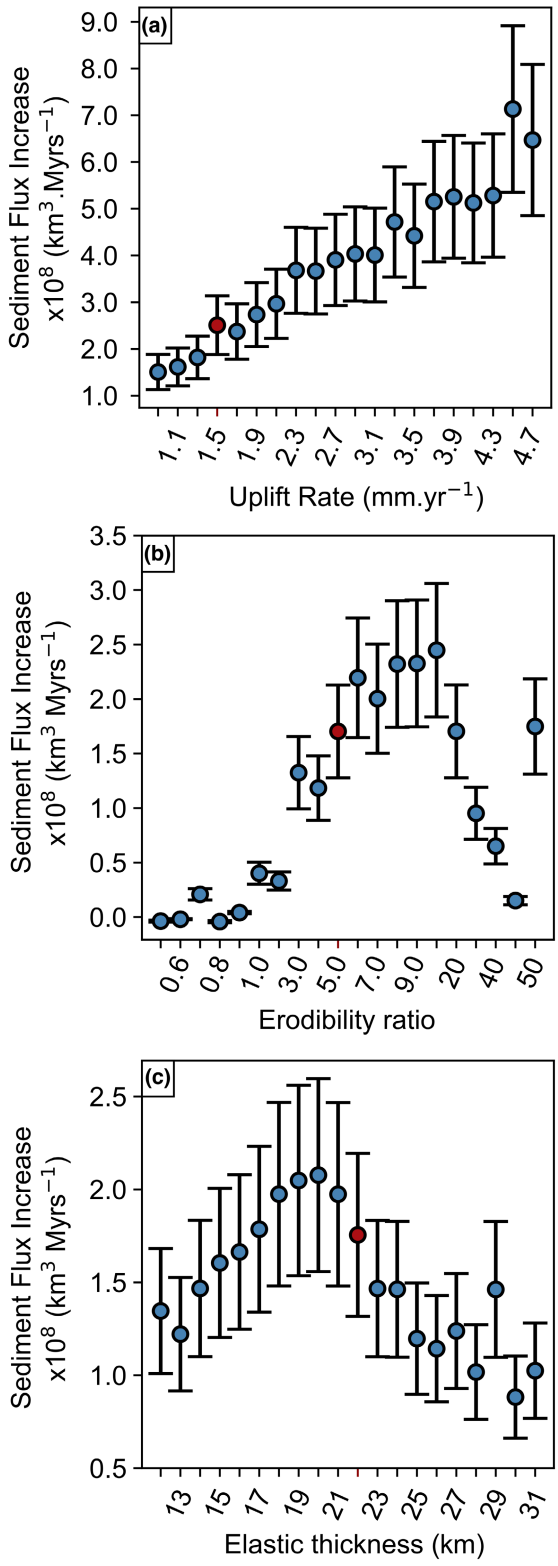

FIGURE 10 Sensitivity analyses on the increase of sediment outflux leaving the system following the post-orogenic transition for different parameters: (a) the uplift rate, (b) the erodibility ratio (K_b / K_m) and (c) the lithosphere elastic thickness. Blue dots and black lines correspond to the model results and uncertainties respectively. Red dots indicate values used for the reference model (i.e. uplift rate: 1.5 mm/year, basin erodibility: 5×10^{-6}, range erodibility: 1×10^{-6} and elastic thickness: 22 km).

sediment outflux following the post-orogenic transition is reached for a lithospheric elastic thickness between 18 and 22 km (Figure 10c); interestingly, this is comparable to the values underlying the NAFB and Aquitaine Basins. Because the elastic flexure has effects on both the range and the basin dynamics, a variation on this parameter will have an important impact on the sediment outflux at the post-orogenic transition. For a stronger lithosphere (i.e. higher lithosphere elastic thickness), the basin flexure will be limited. Therefore, the amount of isostatic rebound and erosion of the basin during post-orogenesis limits the sediment's outflux signal as observed in Figure 10c. However, for a weaker lithosphere (i.e. lower lithosphere elastic thickness), the basement of the basin will have a very pronounced concave form and the basin width is smaller. In this case, the amount of material uplifted will be less important resulting in a limited post-orogenic sediment flux increase (Figure 10c). Maximum sediment outflux increase is reached with a range of lithosphere elastic thickness values that enable both enough isostatic rebound and a sufficient wavelength of rebound to generate the highest sediment yield.

5 | DISCUSSION

5.1 | Basin dynamics during post-orogenesis

The results from the model run to highlight the importance of basin flexure in the evolution of the orogenic system by linking the thrust belt and foreland basin together. Subsidence in the foreland basin induced by the growth of the range and flexure of the lithosphere is more important than the sedimentary influx from the range resulting in all the sediments being trapped in the basin (Figure 11a). This represents the underfilled development of the basin characterised by deep-water marine sedimentation (Covey, 1986; Sinclair, 1997). As the thrust wedge growths and starts to reach steady-state conditions, the sedimentary influx from the range is at a maximum while foreland basin subsidence rates reduce through time. The resulting reduction of accommodation space leads the basin to evolve towards over-filled, continental conditions and allows the development of important fans (Figures 4a and 11b). Post-orogenesis is marked by the cessation of rock uplift in the thrust wedge and a decrease in topography and mass (Figure 5a). The response is a flexural rebound of the lithosphere in order to rebalance the system to the reduced surface topography. The lithospheric rebound is represented in the foreland basin by a surface uplift mainly located in the proximal part of the basin.

13652117, 0, Downloaded from https://onlinelibrary.wiley.com/doi/10.1111/bre.12727 by Universite De Rennes 1, Wiley Online Library on [08/11/2022]. See the Terms and Conditions (https://onlinelibrary.wiley.com/terms-and-conditions) on Wiley Online Library for rules of use; OA articles are governed by the applicable Creative Commons License

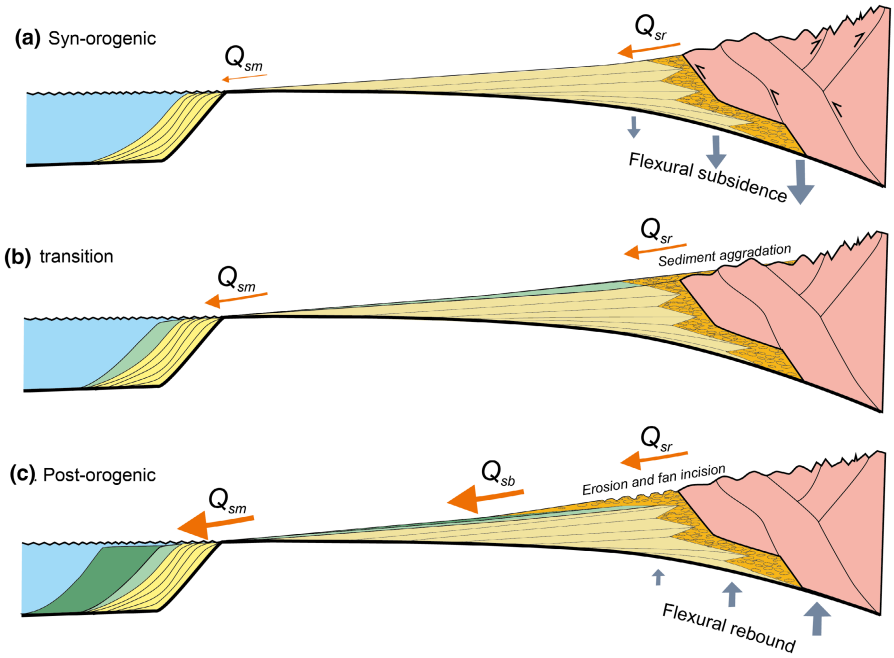

FIGURE 11 Schematic figure highlighting the source-to-sink processes of a thrust wedge, foreland basin and distal depocenter system coupled by flexural isostasy during (a) Syn-orogenesis, (b) the transition and (c) post-orogenesis. Waves on the proximal part of the basin indicate important erosion occurring during the post-orogenic phase. Q_{sm} is the flux to the marine setting, Q_{sb} is the flux from the basin and Q_{sr} is the flux from the range. The size of the arrows qualitatively illustrates the changes in relative flux within the system. The erosional flux from the basin (Q_{sb}) only becomes relevant during the post-orogenic period where it combines with the range flux to increase the marine flux to continental margins.

The combination of isostatic rebound and high sediment yield from the range results in a significant increase in the surface elevation of the foreland basin (Figure 6). As topography increases in the foreland basin due to flexural rebound, the proximal part of the basin switches to an erosional state characterised by channel incisions (Figures 4a and 7g–l).

These features are equally observed in the modern topography, especially at the Lannemezan fan of the Aquitaine Basin (Figure 2c). Because of the difference in flexural rebound across the basin, the location of sediment accumulation migrates towards the distal part of the foreland basin forming an unconformity characterised by stratigraphic offlap (Christie-Blick, 1991) (Figure 11). This pattern should be reflected in natural settings by the exposure of older post-orogenic sediments in the proximal part of the basin and younger post-orogenic sediments in the distal parts of the basin. This transition of a basin dominated by deposition to one of erosion allows the combination of material coming from the erosion of the range and from the basin and is responsible for the increase of sediment flux towards surrounding continental margins (Figures 9 and 11c). In the latter post-orogenic stage, the whole foreland basin switches to erosion (Figure 8e–l) along with a progressive diminution of elevation (Figure 5d) and sediment outflux (Figure 9).

5.2 | Comparison with the Western Alps and Northern Pyrenees

The first-order behaviour of orogenic systems is the temporal relationship between the cessation of tectonic activity in the mountain range, the switch from deposition to erosion in the foreland basin and the increase of sediment flux to distal depocentres. This trend is observed in both natural settings (Figures 1 and 2) and in our simulation (Figure 9). However, it is important to note that this exercise was not an attempt to simulate these systems, but to evaluate whether their development is consistent with the model predictions. Other factors such as local tectonics, dynamic topography and climate undoubtedly influence these settings during their orogenic decline.

Driving mechanisms for the late evolution of the NAFB have been extensively studied (Cederbom et al., 2004; Willett et al., 2006). Erosion of the NAFB has been recorded by mineral cooling ages around 5 Ma which coincide with the decline of structural deformation in the Western European Alps (Cederbom et al., 2004). They also proposed that a wetter climate, induced by the intensification of the Gulf Stream in the Atlantic at 4.6 Ma, may have enhanced the unroofing of the Alps and therefore, the isostatic rebound in the NAFB (Cederbom et al., 2004). Cederbom et al. (2011) suggested that an increase in precipitation combined with a

13652117, 0, Downloaded from https://onlinelibrary.wiley.com/doi/10.1111/bre.12727 by Universite De Rennes 1, Wiley Online Library on [08/11/2022]. See the Terms and Conditions (https://onlinelibrary.wiley.com/terms-and-conditions) on Wiley Online Library for rules of use; OA articles are governed by the applicable Creative Commons License

drainage reorganisation to explain the recorded erosion pattern in the NAFB and Alpine orogen. Other processes such as underplating or mantle dynamics have also been used to explain changes in sediment flux and erosion rates in the Western Alps (Fox et al., 2015; Kuhlemann et al., 2002). Although revisions have been made to our understanding of the lithospheric slab beneath the Alps that may impact these interpretations (Handy et al., 2021). A later increase of sediment accumulation rates since ca. 3 Ma coincides with the global late Pliocene temperature drop. Acceleration of erosion due to Alpine glaciation is likely to play a role in this (Kuhlemann et al., 2002; Valla et al., 2012). But for all these theories, the post-orogenic acceleration of sediment flux from the Western Alps combined with the rebound of the NAFB has to be accounted for prior to the external forcings outlined above.

In the Aquitaine Basin, records of erosion are less well documented. Modelling of low-temperature thermochronological data sets in the proximal part of the basin does not record major cooling following the syn- to post-orogenic transition (Bosch, 2016). This is best explained by a limited amount of erosion in the basin that cannot be detected by the isotopic systems used (i.e. apatite fission track and apatite helium). However, the basin stratigraphy indicates a period of bypass during Aquitanian and Burdigalian times that coincide with the transition to post-orogenesis in the range (Ortiz et al., 2020). Ortiz et al. (2020) also suggest that a West European scale deformation uplifted the basin during the middle to late Miocene enhancing this trend. As with the Western Alps, we suggest that a significant part of this signal can be interpreted as a result of post-orogenic rebound of the mountain belt and foreland basin.

5.3 | Model limitations

The model presents several limitations and cannot replicate some processes that occur during the evolution of an orogenic thrust wedge. For example, our model assumes a system characterised by transport-limited erosion. Previous studies have shown that a transition from detachment- to transport-limited condition is expected during topographic decay (Whipple & Tucker, 2002). This transition can be responsible for longer topographic survival and more uniform erosion preserving topography all along the catchment (Baldwin et al., 2003). Partial protection of the bedrock channel floor by an alluvial cover during transport-limited conditions inhibits erosion. In our model, it can be related to a decrease in the erodibility in the mountain range. A reduction of the range topographic decay will reduce the flexural rebound of the system and therefore erosion in the basin.

Our model approach does not account for regional rock uplift induced by mantle dynamics that may impact both mountain and basin topography (e.g. Faccenna et al., 2014). Additional loads on the downgoing slab may also increase the flexure of the foreland basin (e.g. Royden & Karner, 1984). The signal observed in this study can be impacted depending on the spatial extent of earlier phases of slab detachment.

6 | CONCLUSION

Numerical modelling of an orogenic system that evolves from syn- to post-orogenesis demonstrates increases in sediment flux leaving the system starting at the transition and lasting for a few millions of years during the initial period following post-orogenesis. We demonstrate that this increase in sediment flux to continental margins can be attributed to the intrinsic evolution of an orogenic system driven by fundamental interactions between the thrust wedge and foreland basin coupled with isostatic flexure. Changes in external forcings such as climate or dynamic topography are not required to initiate higher sediment outflux during this period. The mechanisms that drive the higher sediment flux can be summarised as follows: (1) The range topography decays during post-orogenesis resulting in an isostatic rebound of the entire mountain range/foreland basin system. (2) A reduction of accommodation space in the foreland basin is followed by surface uplift that leads to a switch from a basin dominated by deposition to erosion. (3) The combination of sediment yield from erosion of a high mountain range as well as the uplifted basin causes higher sediment flux and accumulation in distal depocentres. Experiments show that in specific, but commonly occurring parameter conditions, an increase of sediment outflux leaving the system can be observed. For example, the erodibility of the basin has to be high relative to the range in order to generate an increase in sediment outflux. In the unusual case of the range being more erodible than the basin, the signal from the basin is overwhelmed by the range signal (which decreases during post-orogenesis) and the increase of sediment outflux at the post-orogenic transition is limited. Similarly, there is an optimal range of values of the lithosphere elastic thickness for the system to encourage higher post-orogenic sediment accumulation. For both the Western European Alps and Northern Pyrenees, accumulation records show a cessation of sediment deposition in their foreland basins while their distal depocentres (The Rhône Delta in the Alps and the Garonne margin for the Pyrenees) experience an increase of sediment accumulation. Several studies have invoked external forcings such as mantle processes or climate to explain these variations in sediment

13652117, 0, Downloaded from https://onlinelibrary.wiley.com/doi/10.1111/bre.12727 by Universite De Rennes 1, Wiley Online Library on [08/11/2022]. See the Terms and Conditions (https://onlinelibrary.wiley.com/terms-and-conditions) on Wiley Online Library for rules of use; OA articles are governed by the applicable Creative Commons License

flux; we conclude that accelerated sediment flux from the combined mountain belt and foreland basin following the syn- to post-orogenic transition needs to be accounted for before additional forces are evoked.

ACKNOWLEDGEMENTS

We thank the OROGEN project, a TOTAL-BRGM-CNRS consortium, for supporting this study. We thank Cari Johnson for editorial support and Sean Willett and two anonymous reviewers for constructive comments, which improved the manuscript.

CONFLICT OF INTEREST

The authors declare that they have no conflict of interest.

PEER REVIEW

The peer review history for this article is available at https://publons.com/publon/10.1111/bre.12727.

DATA AVAILABILITY STATEMENT

The data that support the findings of this study are available from the corresponding author upon reasonable request.

ORCID

Thomas Bernard https://orcid.org/0000-0002-3230-4629

REFERENCES

Allen, P. A. (2008). Time scales of tectonic landscapes and their sediment routing systems. *Geological Society, London, Special Publications*, *296*(1), 7–28. https://doi.org/10.1144/sp296.2

Allen, P. A., Armitage, J. J., Carter, A., Duller, R. A., Michael, N. A., Sinclair, H. D., Whitchurch, A. L., & Whittaker, A. C. (2013). The Qsproblem: Sediment volumetric balance of proximal foreland basin systems. *Sedimentology*, *60*(1), 102–130. https://doi.org/10.1111/sed.12015

Allen, P. A., Crampton, S. L., & Sinclair, H. D. (1991). The inception and early evolution of the north Alpine foreland basin, Switzerland. *Basin Research*, *3*(3), 143–163. https://doi.org/10.1111/j.1365-2117.1991.tb00124.x

Baldwin, J. A., Whipple, K. X., & Tucker, G. E. (2003). Implications of the shear stress river incision model for the timescale of postorogenic decay of topography. *Journal of Geophysical Research: Solid Earth*, *108*(B3). https://doi.org/10.1029/2001jb000550

Baran, R., Friedrich, A. M., & Schlunegger, F. (2014). The late Miocene to Holocene erosion pattern of the Alpine foreland basin reflects Eurasian slab unloading beneath the western Alps rather than global climate change. *Lithosphere*, *6*(2), 124–131. https://doi.org/10.1130/L307.1

Beaumont, C. (1981). Foreland basins. *Geophysical Journal of the Royal Astronomical Society*, *65*(2), 291–329. https://doi.org/10.1111/j.1365-246X.1981.tb02715.x

Bernard, T., Sinclair, H. D., Naylor, M., Christophoul, F., & Ford, M. (2021). Post-orogenic sediment drape in the Northern Pyrenees explained using a box model. *Basin Research*, *33*(1), 118–137. https://doi.org/10.1111/bre.12457

Biteau, J.-J., Le Marrec, A., Le Vot, M., & Masset, J.-M. (2006). The Aquitaine Basin. *Petroleum Geoscience*, *6*(2), 295–306. https://doi.org/10.1144/1354-079305-674

i Bosch, V. (2016). *Pénéplanation et dynamique de la lithosphère dans les Pyrénées* (Doctoral dissertation, Rennes 1).

Bourrouilh, R., Richert, J. P., & Zolnai, G. (1995). The north Pyrenean Aquitaine Basin, France: Evolution and hydrocarbons. *American Association of Petroleum Geologists Bulletin*, *79*(6), 831–853. https://doi.org/10.1306/8D2B1BC4-171E-11D7-8645000102C1865D

Bovy, B. (2020). fastscape-lem/fastscape 0.1.0beta (Version 0.1.0beta). *Zenodo*.

Braun, J., Simon-Labric, T., Murray, K. E., & Reiners, P. W. (2014). Topographic relief driven by variations in surface rock density. *Nature Geoscience*, *7*(7), 534–540. https://doi.org/10.1038/ngeo2171

Braun, J., & Willett, S. D. (2013). A very efficient O(n), implicit and parallel method to solve the stream power equation governing fluvial incision and landscape evolution. *Geomorphology*, *180*, 170–179. https://doi.org/10.1016/j.geomorph.2012.10.008

Brunet, M. F. (1986). The influence of the evolution of the Pyrenees on adjacent basins. *Tectonophysics*, *129*(1–4), 343–354. https://doi.org/10.1016/0040-1951(86)90260-X

Cederbom, C. E., Sinclair, H. D., Schlunegger, F., & Rahn, M. K. (2004). Climate-induced rebound and exhumation of the European Alps. *Geology*, *32*(8), 709–712. https://doi.org/10.1130/G20491.1

Cederbom, C. E., Van Der Beek, P., Schlunegger, F., Sinclair, H. D., & Oncken, O. (2011). Rapid extensive erosion of the North Alpine foreland basin at 5-4Ma. *Basin Research*, *23*(5), 528–550. https://doi.org/10.1111/j.1365-2117.2011.00501.x

Christie-Blick, N. (1991). Onlap, offlap, and the origin of unconformity-bounded depositional sequences. *Marine Geology*, *97*(1–2), 35–56. https://doi.org/10.1016/0025-3227(91)90018-Y

Clift, P. D. (2006). Controls on the erosion of Cenozoic Asia and the flux of clastic sediment to the ocean. *Earth and Planetary Science Letters*, *241*(3–4), 571–580. https://doi.org/10.1016/j.epsl.2005.11.028

Covey, M. (1986). The evolution of foreland basins to steady state: Evidence from the western Taiwan foreland basin. *Foreland Basins*, 77–90. https://doi.org/10.1002/9781444303810.ch4

Curry, M. E., van der Beek, P., Huismans, R. S., Wolf, S. G., & Muñoz, J. A. (2019). Evolving paleotopography and lithospheric flexure of the Pyrenean orogen from 3D flexural modeling and basin analysis. *Earth and Planetary Science Letters*, *515*, 26–37. https://doi.org/10.1016/j.epsl.2019.03.009

Debroas, E. J. (1990). Le Flysch noir albo-cenomanien témoin de la structuration albienne à sénonienne de la Zone nord-pyrénéenne en Bigorre (Hautes-Pyrénées, France). *Bulletin de la Société géologique de France*, *6*(2), 273–285. https://doi.org/10.2113/gssgfbull.vi.2.273

Delunel, R., Schlunegger, F., Valla, P. G., Dixon, J., Glotzbach, C., Hippe, K., Kober, F., Molliex, S., Norton, K. P., Salcher, B., Wittmann, H., Akçar, N., & Christl, M. (2020). Late-Pleistocene catchment-wide denudation patterns across the European Alps. *Earth-Science Reviews*, *211*, 103407. https://doi.org/10.1016/j.earscirev.2020.103407

Desegaulx, P., Roure, F., & Villein, A. (1990). Structural evolution of the Pyrenees: Tectonic inheritance and flexural behaviour

13652117, 0, Downloaded from https://onlinelibrary.wiley.com/doi/10.1111/bre.12727 by Universite De Rennes 1, Wiley Online Library on [08/11/2022]. See the Terms and Conditions (https://onlinelibrary.wiley.com/terms-and-conditions) on Wiley Online Library for rules of use; OA articles are governed by the applicable Creative Commons License

in the continental crust. *Tectonophysics*, *182*(3–4), 211–225. https://doi.org/10.1016/0040-1951(90)90164-4

Faccenna, C., Becker, T. W., Auer, L., Billi, A., Boschi, L., Brun, J. P., Capitanio, F. A., Funiciello, F., Horvàth, F., Jolivet, L., Piromallo, C., Royden, L., Rossetti, F., & Serpelloni, E. (2014). Mantle dynamics in the Mediterranean. *Reviews of Geophysics*, *52*, 283–332. https://doi.org/10.1002/2013RG000444

Fillon, C., Mouthereau, F., Calassou, S., Pik, R., Bellahsen, N., Gautheron, C., Stockli, D., Brichau, S., Daril, N., Mouchené, M., & van der Beek, P. (2021). Post-orogenic exhumation in the western pyrenees: Evidence for extension driven by pre-orogenic inheritance. *Journal of the Geological Society*, *178*(2). https://doi.org/10.1144/jgs2020-079

Fitzgerald, P. G., Muñoz, J. A., Coney, P. J., & Baldwin, S. L. (1999). Asymmetric exhumation across the Pyrenean orogen: Implications for the tectonic evolution of a collisional orogen. *Earth and Planetary Science Letters*, *173*(3), 157–170. https://doi.org/10.1016/S0012-821X(99)00225-3

Flemings, P. B., & Jordan, T. E. (1989). A synthetic stratigraphic model of foreland basin development. *Journal of Geophysical Research*, *94*(B4), 3851–3866. https://doi.org/10.1029/JB094iB04p03851

Ford, M., Hemmer, L., Vacherat, A., Gallagher, K., & Christophoul, F. (2016). Retro-wedge foreland basin evolution along the ECORS line, eastern Pyrenees, France. *Journal of the Geological Society*, *173*(3), 419–437. https://doi.org/10.1144/jgs2015-129

Fox, M., Herman, F., Kissling, E., & Willett, S. D. (2015). Rapid exhumation in the Western Alps driven by slab detachment and glacial erosion. *Geology*, *53*(5), 379–382. https://doi.org/10.1130/G36411.1

Gallen, S. F. (2018). Lithologic controls on landscape dynamics and aquatic species evolution in post-orogenic mountains. *Earth and Planetary Science Letters*, *493*, 150–160. https://doi.org/10.1016/j.epsl.2018.04.029

Gardère, P., Rey, J., & Duranthon, F. (2002). Les «Sables fauves», témoins de mouvements tectoniques dans le bassin d'Aquitaine au Miocène moyen. *Comptes Rendus Geoscience*, *334*(13), 987–994. https://doi.org/10.1016/s1631-0713(02)01844-8

Gibson, M., Sinclair, H. D., Lynn, G. J., & Stuart, F. M. (2007). Late- to post-orogenic exhumation of the Central Pyrenees revealed through combined thermochronological data and modelling. *Basin Research*, *19*(3), 323–334. https://doi.org/10.1111/j.1365-2117.2007.00333.x

Guerit, L., Yuan, X. P., Carretier, S., Bonnet, S., Rohais, S., Braun, J., & Rouby, D. (2019). Fluvial landscape evolution controlled by the sediment deposition coefficient: Estimation from experimental and natural landscapes. *Geology*, *47*(9), 853–856. https://doi.org/10.1130/G46356.1

Handy, M. R., Schmid, S. M., Paffrath, M., & Friederich, W. (2021). Orogenic lithosphere and slabs in the greater Alpine area—Interpretations based on teleseismic P-wave tomography. *Solid Earth*, *12*(11), 2633–2669. https://doi.org/10.5194/se-12-2633-2021

Homewood, P., Allen, P. A., & Williams, G. D. (1986). Dynamics of the Molasse Basin of western Switzerland. *Foreland Basins*, *8*, 199–217. https://doi.org/10.1002/9781444303810.ch10

Jamieson, R. A., & Beaumont, C. (1988). Orogeny and metamorphism: A model for deformation and pressure-temperature-time paths with applications to the central and southern Appalachians. *Tectonics*, *7*(3), 417–445. https://doi.org/10.1029/TC007i003p00417

Jolivet, M., Labaume, P., Monié, P., Brunel, M., Arnaud, N., & Campani, M. (2007). Thermochronology constraints for the propagation sequence of the south Pyrenean basement thrust system (France-Spain). *Tectonics*, *26*(5). https://doi.org/10.1029/2006TC002080

Karner, G. D., & Watts, A. B. (1983). Gravity anomalies and flexure of the lithosphere at mountain ranges. *Journal of Geophysical Research*, *88*(B12), 10449–10477. https://doi.org/10.1029/JB088iB12p10449

Kirby, E., & Whipple, K. X. (2012). Expression of active tectonics in erosional landscapes. *Journal of Structural Geology*, *44*, 54–75. https://doi.org/10.1016/j.jsg.2012.07.009

Kuhlemann, J., Frisch, W., Dunkl, I., & Székely, B. (2001). Quantifying tectonic versus erosive denudation by the sediment budget: The miocene core complexes of the Alps. *Tectonophysics*, *330*(1–2), 1–23. https://doi.org/10.1016/S0040-1951(00)00209-2

Kuhlemann, J., Frisch, W., Székely, B., Dunkl, I., & Kázmér, M. (2002). Post-collisional sediment budget history of the Alps: Tectonic versus climatic control. *International Journal of Earth Sciences*, *91*(5), 818–837. https://doi.org/10.1007/s00531-002-0266-y

Kuhlemann, J., & Kempf, O. (2002). Post-Eocene evolution of the North Alpine Foreland Basin and its response to Alpine tectonics. *Sedimentary Geology*, *152*(1–2), 45–78. https://doi.org/10.1016/S0037-0738(01)00285-8

Lupker, M., France-Lanord, C., Lavé, J., Bouchez, J., Galy, V., Métivier, F., Gaillardet, J., Lartiges, B., & Mugnier, J. L. (2011). A Rouse-based method to integrate the chemical composition of river sediments: Application to the Ganga basin. *Journal of Geophysical Research: Earth Surface*, *116*(F4). https://doi.org/10.1029/2010JF001947

Madritsch, H., Preusser, F., Fabbri, O., Bichet, V., Schlunegger, F., & Schmid, S. M. (2010). Late quaternary folding in the Jura Mountains: Evidence from syn-erosional deformation of fluvial meanders. *Terra Nova*, *22*(2), 147–154. https://doi.org/10.1111/j.1365-3121.2010.00928.x

Martel, A. T., Allen, P. A., & Slingerland, R. (1994). Use of tidal-circulation modeling in paleogeographical studies: An example from the Tertiary of the Alpine perimeter. *Geology*, *22*(10), 925–928. https://doi.org/10.1130/0091-7613(1994)022<0925:UOTCMI>2.3.CO;2

Meigs, A. J., Vergés, J., & Burbank, D. W. (1996). Ten-million-year history of a thrust sheet. *Bulletin of the Geological Society of America*, *108*(12), 1608–1625. https://doi.org/10.1130/0016-7606(1996)108<1608:TMYHOA>2.3.CO;2

Milliman, J. D., & Farnsworth, K. L. (2011). *River discharge to the coastal ocean: A global synthesis*. Cambridge University Press. https://doi.org/10.1017/CBO9780511781247

Molnar, P. (2004). Late Cenozoic increase in accumulation rates of terrestrial sediment: How might climate change have affected erosion rates? *Annual Review of Earth and Planetary Sciences*, *32*, 67–89. https://doi.org/10.1146/annurev.earth.32.091003.143456

Morris, R. G., Sinclair, H. D., & Yelland, A. J. (1998). Exhumation of the Pyrenean orogen: Implications for sediment discharge. *Basin Research*, *10*(1), 69–86. https://doi.org/10.1046/j.1365-2117.1998.00053.x

13652117, 0, Downloaded from https://onlinelibrary.wiley.com/doi/10.1111/bre.12727 by Universite De Rennes 1, Wiley Online Library on [08/11/2022]. See the Terms and Conditions (https://onlinelibrary.wiley.com/terms-and-conditions) on Wiley Online Library for rules of use; OA articles are governed by the applicable Creative Commons License

Naylor, M., & Sinclair, H. D. (2008). Pro- vs. retro-foreland basins. *Basin Research*, *20*(3), 285–303. https://doi.org/10.1111/j.1365-2117.2008.00366.x

Nocquet, J. M., & Calais, E. (2003). Crustal velocity field of western Europe from permanent GPS array solutions, 1996-2001. *Geophysical Journal International*, *154*(1), 72–88. https://doi.org/10.1046/j.1365-246X.2003.01935.x

Ortiz, A., Guillocheau, F., Lasseur, E., Briais, J., Robin, C., Serrano, O., & Fillon, C. (2020). Sediment routing system and sink preservation during the post-orogenic evolution of a retro-foreland basin: The case example of the North Pyrenean (Aquitaine, Bay of Biscay) Basins. *Marine and Petroleum Geology*, *112*, 104085. https://doi.org/10.1016/j.marpetgeo.2019.104085

Ortiz, A., Guillocheau, F., Robin, C., Lasseur, E., Briais, J., & Fillon, C. (2022). Siliciclastic sediment volumes and rates of the North Pyrenean retro-foreland basin. *Basin Research.*, *34*, 1421–1439. https://doi.org/10.1111/bre.12665

Pazzaglia, F. J., & Brandon, M. T. (1996). Macrogeomorphic evolution of the post-Triassic Appalachian mountains determined by deconvolution of the offshore basin sedimentary record. *Basin Research*, *8*(3), 255–278. https://doi.org/10.1046/j.1365-2117.1996.00274.x

Peizhen, Z., Molnar, P., & Downs, W. R. (2001). Increased sedimentation rates and grain sizes 2-4 Myr ago due to the influence of climate change on erosion rates. *Nature*, *410*(6831), 891–897. https://doi.org/10.1038/35073504

Pfiffner, O. A. (1986). Evolution of the North Alpine Foreland Basin in the Central Alps. *Foreland Basins*, *38*(6), 570–576. https://doi.org/10.1002/9781444303810.ch11

Roest, W. R., & Srivastava, S. P. (1991). Kinematics of the plate boundaries between Eurasia, Iberia, and Africa in the North Atlantic from the Late Cretaceous to the present. *Geology*, *19*(6), 613–616. https://doi.org/10.1130/0091-7613(1991)019<0613:KOTPBB>2.3.CO;2

Rougier, G., Ford, M., Christophoul, F., & Bader, A. G. (2016). Stratigraphic and tectonic studies in the Central Aquitaine Basin, northern Pyrenees: Constraints on the subsidence and deformation history of a retro-foreland basin. *Comptes Rendus—Geoscience*, *348*(3–4), 224–235. https://doi.org/10.1016/j.crte.2015.12.005

Royden, L. H., & Karner, G. D. (1984). Flexure of the continental lithosphere beneath Apennine and Carpathian foredeep basins. *Nature*, *309*(5964), 142–144. https://doi.org/10.1038/309142a0

Sadler, P. M. (1981). Sediment accumulation rates and the completeness of stratigraphic sections. *Journal of Geology*, *89*(5), 569–584. https://doi.org/10.1086/628623

Schlunegger, F., Matter, A., Burbank, D. W., Leu, W., Mange, M., & Màtyàs, J. (1997). Sedimentary sequences, seismofacies and evolution of depositional systems of the Oligo/Miocene Lower Freshwater Molasse Group, Switzerland. *Basin Research*, *9*(1), 1–26. https://doi.org/10.1046/j.1365-2117.1997.00029.x

Schlunegger, F., & Mosar, J. (2011). The last erosional stage of the Molasse Basin and the Alps. *International Journal of Earth Sciences*, *100*(5), 1147–1162. https://doi.org/10.1007/s00531-010-0607-1

Schmid, S. M., Fügenschuh, B., Kissling, E., & Schuster, R. (2004). Tectonic map and overall architecture of the Alpine orogen. *Eclogae Geologicae Helvetiae*, *97*(1), 93–117. https://doi.org/10.1007/s00015-004-1113-x

Sinclair, H. D. (1997). Tectonostratigraphic model for underfilled peripheral foreland basins: An Alpine perspective. *Bulletin of the Geological Society of America*, *109*(3), 324–346. https://doi.org/10.1130/0016-7606(1997)109<0324:TMFUPF>2.3.CO;2

Sinclair, H. D., & Allen, P. A. (1992). Vertical versus horizontal motions in the Alpine orogenic wedge: Stratigraphic response in the foreland basin. *Basin Research*, *4*(3–4), 215–232. https://doi.org/10.1111/j.1365-2117.1992.tb00046.x

Sinclair, H. D., Coakley, B. J., Allen, P. A., & Watts, A. B. (1991). Simulation of Foreland Basin stratigraphy using a diffusion model of mountain belt uplift and erosion: An example from the Central Alps, Switzerland. *Tectonics*, *10*(3), 599–620. https://doi.org/10.1029/90TC02507

Sinclair, H. D., Gibson, M., Naylor, M., & Morris, R. G. (2005). Asymmetric growth of the Pyrenees revealed through measurement and modeling of orogenic fluxes. *American Journal of Science*, *305*(5), 369–406. https://doi.org/10.2475/ajs.305.5.369

Sinclair, H. D., Stuart, F. M., Mudd, S. M., McCann, L., & Tao, Z. (2019). Detrital cosmogenic ^{21}Ne records decoupling of source-to-sink signals by sediment storage and recycling in Miocene to present rivers of the Great Plains, Nebraska, USA. *Geology*, *47*(1), 3–6. https://doi.org/10.1130/G45391.1

Sternai, P., Sue, C., Husson, L., Serpelloni, E., Becker, T. W., Willett, S. D., Faccenna, C., di Giulio, A., Spada, G., Jolivet, L., Valla, P., Petit, C., Nocquet, J. M., Walpersdorf, A., & Castelltort, S. (2019). Present-day uplift of the European Alps: Evaluating mechanisms and models of their relative contributions. *Earth-Science Reviews*, *190*, 589–604. https://doi.org/10.1016/j.earscirev.2019.01.005

Sue, C., Delacou, B., Champagnac, J. D., Allanic, C., Tricart, P., & Burkhard, M. (2007). Extensional neotectonics around the bend of the Western/Central Alps: An overview. *International Journal of Earth Sciences*, *96*(6), 1101–1129. https://doi.org/10.1007/s00531-007-0181-3

Syvitski, J. P. M., & Milliman, J. D. (2007). Geology, geography, and humans battle for dominance over the delivery of fluvial sediment to the coastal ocean. *Journal of Geology*, *115*(1), 1–19. https://doi.org/10.1086/509246

Syvitski, J. P. M., & Saito, Y. (2007). Morphodynamics of deltas under the influence of humans. *Global and Planetary Change*, *57*(3–4), 261–282. https://doi.org/10.1016/j.gloplacha.2006.12.001

Tucker, G. E., & Slingerland, R. (1996). Predicting sediment flux from fold and thrust belts. *Basin Research*, *8*(3), 329–349. https://doi.org/10.1046/j.1365-2117.1996.00238.x

Tucker, G. E., & van der Beek, P. (2013). A model for post-orogenic development of a mountain range and its foreland. *Basin Research*, *25*(3), 241–259. https://doi.org/10.1111/j.1365-2117.2012.00559.x

Valla, P. G., van der Beek, P. A., Shuster, D. L., Braun, J., Herman, F., Tassan-Got, L., & Gautheron, C. (2012). Late Neogene exhumation and relief development of the Aar and Aiguilles Rouges massifs (Swiss Alps) from low-temperature thermochronology modeling and 4He/3He thermochronometry. *Journal of Geophysical Research: Earth Surface*, *117*(F1). https://doi.org/10.1029/2011JF002043

von Hagke, C., Oncken, O., Ortner, H., Cederbom, C. E., & Aichholzer, S. (2014). Late Miocene to present deformation and erosion of the Central Alps—Evidence for steady state mountain building from thermokinematic data. *Tectonophysics*, *632*, 250–260. https://doi.org/10.1016/j.tecto.2014.06.021

Whipple, K. X. (2009). The influence of climate on the tectonic evolution of mountain belts. *Nature Geoscience*, *2*(2), 97–104. https://doi.org/10.1038/ngeo413

13652117, 0, Downloaded from https://onlinelibrary.wiley.com/doi/10.1111/bre.12727 by Universite De Rennes 1, Wiley Online Library on [08/11/2022]. See the Terms and Conditions (https://onlinelibrary.wiley.com/terms-and-conditions) on Wiley Online Library for rules of use; OA articles are governed by the applicable Creative Commons License

Whipple, K. X., & Tucker, G. E. (1999). Dynamics of the stream-power river incision model: Implications for height limits of mountain ranges, landscape response timescales, and research needs. *Journal of Geophysical Research: Solid Earth*, *104*(B8), 17661–17674. https://doi.org/10.1029/1999jb900120

Whipple, K. X., & Tucker, G. E. (2002). Implications of sediment-flux-dependent river incision models for landscape evolution. *Journal of Geophysical Research*, *107*(B2), ETG-3. https://doi.org/10.1029/2000jb000044

Willenbring, J. K., & Jerolmack, D. J. (2016). The null hypothesis: Globally steady rates of erosion, weathering fluxes and shelf sediment accumulation during Late Cenozoic mountain uplift and glaciation. *Terra Nova*, *28*(1), 11–18. https://doi.org/10.1111/ter.12185

Willett, S. D. (2010). Late neogene erosion of the alps: A climate driver? *Annual Review of Earth and Planetary Sciences*, *38*, 411–437. https://doi.org/10.1146/annurev-earth-040809-152543

Willett, S. D., & Brandon, M. T. (2002). On steady states in mountain belts. *Geology*, *30*(2), 175–178. https://doi.org/10.1130/0091-7613(2002)030<0175:OSSIMB>2.0.CO;2

Willett, S. D., Schlunegger, F., & Picotti, V. (2006). Messinian climate change and erosional destruction of the central European Alps. *Geology*, *34*(8), 613–616. https://doi.org/10.1130/G22280.1

Winterberg, S., & Willett, S. D. (2019). Greater Alpine river network evolution, interpretations based on novel drainage analysis. *Swiss Journal of Geosciences*, *112*(1), 3–22. https://doi.org/10.1007/s00015-018-0332-5

Wittmann, H., Malusà, M. G., Resentini, A., Garzanti, E., & Niedermann, S. (2016). The cosmogenic record of mountain erosion transmitted across a foreland basin: Source-to-sink analysis of in situ 10Be, 26Al and ^{21}Ne in sediment of the Po river catchment. *Earth and Planetary Science Letters*, *452*, 258–271. https://doi.org/10.1016/j.epsl.2016.07.017

Wittmann, H., von Blanckenburg, F., Kruesmann, T., Norton, K. P., & Kubik, P. W. (2007). Relation between rock uplift and denudation from cosmogenic nuclides in river sediment in the Central Alps of Switzerland. *Journal of Geophysical Research: Earth Surface*, *112*(F4). https://doi.org/10.1029/2006JF000729

Wittmann, H., von Blanckenburg, F., Maurice, L., Guyot, J. L., & Kubik, P. W. (2011). Recycling of Amazon floodplain sediment quantified by cosmogenic 26Al and 10Be. *Geology*, *39*(5), 467–470. https://doi.org/10.1130/G31829.1

Yuan, X. P., Braun, J., Guerit, L., Rouby, D., & Cordonnier, G. (2019). A new efficient method to solve the stream power law model taking into account sediment deposition. *Journal of Geophysical Research: Earth Surface*, *124*(6), 1346–1365. https://doi.org/10.1029/2018JF004867

Yuan, X. P., Braun, J., Guerit, L., Simon, B., Bovy, B., Rouby, D., Robin, C., & Jiao, R. (2019). Linking continental erosion to marine sediment transport and deposition: A new implicit and O(N) method for inverse analysis. *Earth and Planetary Science Letters*, *524*, 115728. https://doi.org/10.1016/j.epsl.2019.115728

Zondervan, J. R., Stokes, M., Boulton, S. J., Telfer, M. W., & Mather, A. E. (2020). Rock strength and structural controls on fluvial erodibility: Implications for drainage divide mobility in a collisional mountain belt. *Earth and Planetary Science Letters*, *538*, 116221. https://doi.org/10.1016/j.epsl.2020.116221

How to cite this article: Bernard, T., & Sinclair, H. D. (2022). Accelerated sediment delivery to continental margins during post-orogenic rebound of mountain ranges. *Basin Research*, *00*, 1–20. https://doi.org/10.1111/bre.12727

13652117, 0, Downloaded from https://onlinelibrary.wiley.com/doi/10.1111/bre.12727 by Universite De Rennes 1, Wiley Online Library on [08/11/2022]. See the Terms and Conditions (https://onlinelibrary.wiley.com/terms-and-conditions) on Wiley Online Library for rules of use; OA articles are governed by the applicable Creative Commons License